A COHERENT OPTICAL EQUALIZATION

BASED ON CHANNEL ESTIMATION

by

Hai Wu

Bachelor of Science, Lan Zhou University, 1993

A Thesis Submitted in Partial Fulfilment of
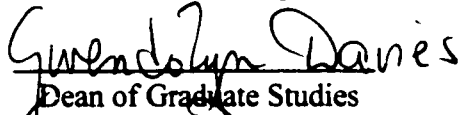the Requirements for the Degree of

Master of Science in Engineering

in the Graduate Academic Unit of Electrical and Computer Engineering

Supervisor: Brent R. Petersen, PhD., Electrical and Computer Engineering

Examining Board: Liuchen Chang, Ph.D., Electrical and Computer Engineering, Chair
Bruce G. Colpitts, Ph.D., Electrical and Computer Engineering
David McG. Luke, M.Sc.Eng., Electrical and Computer Engineering
Richard B. Langley, Ph.D., Geodesy and Geomatics Engineering

This thesis is accepted

Dean of Graduate Studies

THE UNIVERSITY OF NEW BRUNSWICK

September, 2000

Abstract

In recent years the importance of polarization in lightwave systems has grown as a result of two developments. First, the optical amplifier has dramatically increased the optical path lengths with single-mode fiber. Second, polarization effects have become important in that transmitter and receiver technologies have pushed the capacity of optical fiber to its limit, even in relatively short spans. Polarization mode dispersion (PMD) is one of the major limitations for the high capacity of optical fiber systems.

The aim of this thesis is to present an analysis of the impairments due to first-order PMD. Using numerical simulations by correlation, the impulse response of the channel with PMD was computed. The coefficients of equalizers are calculated by the LMS algorithm. The bandwidth of the optical channel is accounted for and fractional-rate tap spacing equalizers are used for compensation. The effect of first-order PMD compensation will be demonstrated using bit error rates and eye diagrams. This method is easy to extend to any order of PMD in optical linear systems.

Acknowledgement

Table of Contents

List of Figures

List of Symbols

$a(n)$	Transmitted data at time n
a_n	Transmitted data at time n
$\tilde{a}(n)$	The received data
A_s	Amplitude of the received optical signal
A_{LO}	Amplitude of the local oscillator
B	Bit rate
B_f	Transmission bandwidth
B_T	Bandwidth
c	Speed of light in the vacuum
c_+	Projection of θ onto fast PSP
c_-	Projection of θ onto slow PSP
$d(n)$	Training data at time n
d_n	Same as $d(n)$
$d(t)$	Known continuous input
$d(-t)$	Time reverse of $d(t)$
$\tilde{d}(n)$	Estimate of data at time n
e	Base of the natural exponential function
e_n	Difference between $d(n)$ and $\tilde{d}(n)$
$e_f(n)$	Channel estimation error
erfc	Complementary error function
eye	The eye opening (in percent)
$e[n]$	Equalizer error
E_a	Electrical signal input to the transmit laser
E_s	Electric field associated with the received optical signal
E_{LO}	Electric field associated with local oscillator
$\overline{E_a}$	Optical input field
$\overline{E_b}$	Optical output field
f	Frequency
f_c	Carrier frequency
f_n	Probability density function of the noise
$g(t)$	Optical signal at the receiver input
$g_h(t)$	Horizontal optical signal at the receiver input
$g_v(t)$	Vertical optical signal at the receiver input
$\hat{g}(t)$	Output optical signal after equalizer
$h_{11}(t)$	Impulse response of the optical co-channel with PMD
$h_{12}(t)$	Impulse response of the optical cross-channel with PMD
$h_{21}(t)$	Impulse response of the optical cross-channel with PMD
$h_{22}(t)$	Impulse response of the optical co-channel with PMD

h(n)	Discrete impulse response of the optical channel with PMD
h(t)	Impulse response of the optical channel with PMD
$h_b(t)$	Baseband impulse response
$h_t(t)$	Impulse response of the transmitter filter
$h_r(n)$	Discrete impulse response of the optical filter
$h_r(t)$	Impulse response of the optical filter
$H_b(f)$	Baseband impulse response in frequency domain
H(f)	Impulse response of the optical channel with PMD in frequency domain
$H_r(f)$	The Fourier transform of the signal $h_r(t)$
$H_T(f)$	The signal spectrum of the T spaced equalizer
$H_{T'}(f)$	The signal spectrum of the T' spaced equalizer
H(z)	Z transform of h(n)
$H_r(z)$	Z transform of $h_r(n)$
h(ω)	Frequence impulse response of the optical channel
$\bar{h}(n)$	Estimate discrete impulse response of the optical channel with PMD
I_d	Dark current
I_p	Current from received optical signal
I(t)	Photocurrent
j	Imaginary number equal to square root of -1
J	Mean square error
k	Integer number
k_B	Boltzmann's constant
K	Number of the waveplate segments
m	Number of taps in optical filter
m1	Number of taps of the optical channel impulse response with PMD
M	Number of frequency samples
$M_k(\omega)$	Jones transfer matrix of the k-th waveplate
n	Indices in time
n_f	Effective index of refraction for the fast mode
n_s	Effective index of refraction for the slow mode
N	Length of training sequences
N1	Length of the sequences used in quasi-analytical method
P_1	Power of the information bearing signal
P_2	Power of the training signal
P_e	Total probability of error
P_k	The probability of error at the k-th sampling instant
P_{out}	Received electrical power
penalty	The optical power penalty
p(k)	Phase shift of the k-th tap of the optical filter
$p(\varphi_k)$	Probability density function of φ_k
PG	Processing gain
q	Electron charge
Q	Ratio of received signal voltage and variance of the noise

R	The responsivity of photodetector
RMS	Normalized RMS width
$R_{dd}(t)$	Auto-correlation of the training sequence
$R_{dy}(t)$	Cross-correlation between the desired sequence d(t) and input of the filter y(t)
R_L	Load resistor
s(t)	Signal at the output of the transmitter
$s_h(t)$	Horizontal optical signal at the output of the transmitter
$s_v(t)$	Vertical optical signal at the output of the transmitter
SNR_I	Input signal-to-noise ratio
SNR_O	Output signal-to-noise ratio
t	Time
1/T	Symbol rate
T	Bit period
T_a	Absolute temperature
T'	Time spacing of fractional spacing equalizer
u(n)	Output after linear system h(n) in calculating equalization coefficients
u_n^T	Matrix transposition of u(n)
$u_1(\omega)$	Elements of a Jones transfer matrix
$u_2(\omega)$	Elements of a Jones transfer matrix
$u_1^*(\omega)$	Complex conjugate of $u_1(\omega)$
$u_2^*(\omega)$	Complex conjugate of $u_2(\omega)$
$U(\omega)$	Jones transfer matrix
v(t)	Interference
v_k	Received electrical value at the k-th sampling instant
w(k)	The k-th tap weight of the optical filter
w_k	The k-th tap weight
$w_r(t)$	Impulse response of the low pass filter
W	Minimum bandwidth
$W_r(f)$	Frequency response of the low pass filter
$\hat{w}_k(n)$	Estimate of $w_k(n)$
S_{dd}	Power spectral density of d(t)
S_{dy}	Cross-spectral density of d(t) and y(t)
y(t)	Output signal used in channel estimation
Y	Difference between the signal levels for a "1" and a "0" without ISI
z	Transmission distance
α	Rolloff factor
β	Complex number
β_f	Propagation constant for the fast mode
β_s	Propagation constant for the slow mode
γ	Power ratio between two PSPs
ϕ_s	Phase of the received optical signal
ϕ_{LO}	Phase of the local oscillator

θ_{in}	Input state of polarization
φ_k	Rotation angle the k-th waveplate
ρ	Fiber loss
$\delta(t)$	Delta function
π	The Ludolphian number, Pi, 3.1415926...
$\langle \eta \rangle$	Mean transmit time
Ψ	Propagation constant
ε	Mean square error
$\overline{\varepsilon}_+$	Output fast principal state of polarization
$\overline{\varepsilon}_-$	Output slow principal state of polarization
τ	Unit delay time used in optical filter
τ_+	Transmission time in the fast eigenmode
τ_-	Transmission time in the slow eigenmode
τ_k	Differential group delay of the k-th waveplate
ω	Angular frequency
ω_c	Carrier frequency
ω_k	The k-th sample frequency
σ	Noise variance
σ_s^2	Shot noise variance
σ_T^2	Thermal noise variance
Δf	Effective noise bandwidth
$\Delta \tau$	Differential group delay
$\Delta \tau_{rms}$	Root mean square of $\Delta \tau$
μ	Step size
*	Convolution
'	Differentiation with respect to angular frequency

List of Abbreviation and Acronyms

BER	Bit error rate
DGD	Differential group delay
EDFA	Erbium Doped Fibre Amplifier
FSE	Fractional spaced equalizer
GHz	Gigahertz
ISI	Intersymbol interference
LMS	Least mean square
NRZ	Non-return to zero
PDF	Probability distribution function
PMD	Polarization mode dispersion
PR	Pseudo random
ps	Picoseconds
PSP	Principal state of polarization
QA	Quasi-analytical
rms	Root mean square
SER	Signal to estimation error ratio
SER'	Normalized signal to estimation error ratio
SNR	Signal to noise ratio
SOP	State of polarization

Chapter 1

INTRODUCTION

1.1 Background and Motivation for This Thesis

With the increasing number of transmission systems operating at 10 Gbit/s channel rate (OC-192) and with the intention to move to 40 Gbit/s rates within the next few years, polarization-mode dispersion (PMD) of the transmission fiber may become one of the limiting effects for high-bit rate transmission due to pulse waveform degradation [1,2], especially when chromatic dispersion is reduced by state-of-the-art techniques like compensating fibers or chirped gratings [5]. Optical amplifiers have dramatically increased the optical length, as a result, small effects such as PMD can accumulate in a span to the point where it becomes an important consideration of lightwave system developers. The second reason that polarization effects have become important is that transmitter and receiver technologies have pushed the capacity of optical fiber to its limit, even in relatively short spans [1]. This has occurred through dramatic increases in bit rates in digital systems. The largest distortions generally arise from first-order PMD, which creates a delayed echo of the original signal in the fiber due to the differential group delay (DGD) of the two principal states of polarization [3]. Though modern single mode fibers exhibit negligible PMD, with average DGD of the order of 0.1 ps/(km$^{1/2}$) [2], some of the older fiber cables can show large PMD effects with average DGD up to 2 ps/(km$^{1/2}$) [2]. Moreover, the instantaneous DGD in such high-PMD fibers generally

fluctuates randomly with time [25,4], and hence can temporarily exceed values of more than 100 ps for transmission distances of only a few hundred kilometers, which may lead to a complete eye closure even in a 10-Gb/s signal [8].

Thus, within the last years, increasing attention has been paid to PMD compensation in general [27] and optical and electrical compensation schemes in detail as it has become evident that some embedded commercial fiber cables may have PMD values unacceptable for certain network scenarios [1]. Assuming negligible polarization dependent loss and no nonlinear effects, Poole proved the existence, at any frequency ω, of a set of two orthogonal states of polarization (SOPs) allowing a convenient decomposition of input and output fields, in other words, light propagation in an optical fiber can be described by a 2×2 complex transfer matrix [3]. He also proved there exist principal states of polarization (PSPs) which have the maximum possible group delay difference (DGD). However, PMD is intricate to tackle because it may vary as a function of time or fiber temperature [25]. Ongoing strategies for reducing PMD in fiber focus on reducing the intrinsic PMD of the fiber by altering the manufacturing process [1]. This has lead to exceptionally low and stable values of PMD in the new generation of single-mode fibers being manufactured. In the optical domain, previous work to compensate PMD has focused on selecting PSPs of the transmission line by input polarization control [51] or implementing a compensator consisting of a small number of DGD sections, separated by polarization transformers [13]. Other optical compensation of first-order PMD is accomplished by introducing a variable time delay between two adjustable or orthogonal polarization states in the optical signal [43]. But residual DGD appears due to

misalignment, if the PSPs vary with the signal wavelength [34]. In the electrical part of an optical receiver, PMD can be equalized by transversal filters [18], since the photocurrent is proportional to the squared field vector magnitude. However, not all PMD distortion can be compensated electronically and it is not bit rate independent [8]. Even if the first order PMD is compensated, the second order is still a problem in some high capacity optical systems [2,15].

In this thesis, a method is proposed using a coherent optical transversal filter [6] based on channel estimation to compensate PMD. Hardware implementations and algorithms will be discussed. The actual simulations are carried out by the software package Matlab and its toolboxes [41]. The aim of the numerical study is to show that this system can achieve PMD compensation and demonstrate the efficiency of this compensator scheme. The major contribution of this thesis is to compensate first-, second-, and higher-order PMD simultaneously.

Often it is difficult to summarize the research of other people in a few sentences since many omissions can occur. It is believed that this summary is sufficient to justify the thesis contributions that follow.

1.2 Thesis Contributions

The contributions described below are PMD analysis and suppression techniques for symbol-rate tap spacing and fractional-rate tap spacing equalizers operating in the presence of PMD and additive white noise.

The first result is the baseband impulse response of a fiber with first order PMD. Jones matrices and birefringent waveplate models are used to simulate PMD.

The second result is that the optical impulse response can be obtained from channel estimation, which will be used to calculate the coefficients of the equalizers.

The third result is that this technique can compensate second-order or even high order PMD not just first-order PMD. The main assumption is that the optical system is a linear system.

The fourth result in this application is that equalizers with taps spaced at fractions of the symbol period will have better performance than equalizers with symbol-rate taps. The difference comes from the excess bandwidth of the transmitted signal.

The fifth result is using an optical transversal filter to compensate PMD which must be done optically because of the large bandwidth used in optical waveguides.

The sixth result is that this method works even when the eye of the received signal is closed.

1.3 Thesis Organization

This description of the thesis organization follows the table of contents.

In chapter 1, the motivation, background, and literature survey put the thesis contributions into perspective. This section describes how this thesis is organized to make those contributions.

Chapter 2 details the model of transmitter, the origins of the PMD, and the optical

transversal filter used to compensate PMD with its large available bandwidth.

Chapter 3 shows the mathematical model of PMD. Based on the waveplate model of PMD, the impulse response of an optical fiber with first-order PMD may be obtained. The eye diagram will be compared before and after the distortion caused by PMD.

In chapter 4, there are discussions through analysis and simulation regarding how to obtain the optical fiber's impulse response by correlation. Bandwidth issues and processing gain will be mentioned. The two types of equalization are symbol-rate tap spacing and fractional-rate tap spacing.

Chapter 5 is concerned with calculating the coefficients of the equalizer and evaluating the performance of equalizers. These evaluations take place in terms of eye diagrams and bit error rate.

In chapter 6 the thesis is concluded, followed by a discussion of potential future work.

Chapter 2
System Model

Fig. 2.1 provides a block diagram of the major components of the optical system: the transmitted data a(n), the transmitter impulse response $h_t(t)$, the impulse response of the fiber with PMD h(t), the interference v(t), and the received data ā(n). The dummy variables t and n denote the indices in time. At the end of this chapter, an optical equalization filter is introduced.

Raised cosine filter   Optical fiber impulse response

$\{a(n)\} \longrightarrow \boxed{h_t(t)} \xrightarrow{s(t)} \boxed{h(t)} \longrightarrow \oplus \xrightarrow{g(t)} \boxed{\text{Receiver}} \longrightarrow \{ā(n)\}$

Transmitted data   Received data
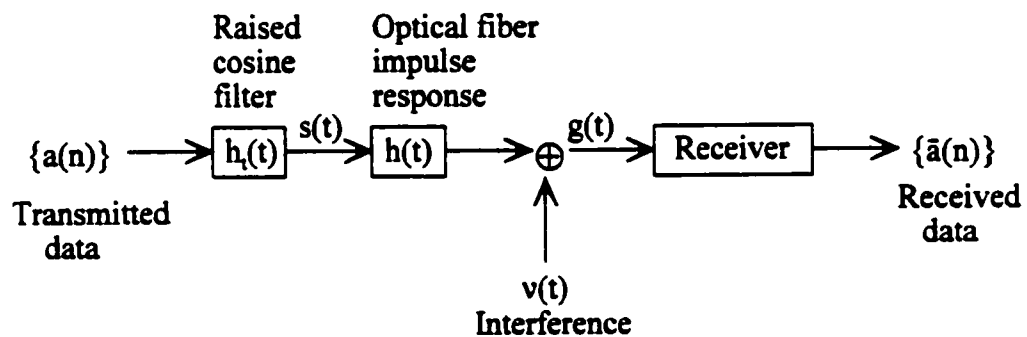
v(t)
Interference

Figure 2.1 Optical System Model

2.1 Transmitter

A variety of signal generators and line coders are used to modulate optical sources [16]. The input data is a random data sequence, possibly coded to achieve a particular

spectral shaping. For this thesis, the simulations are driven using pseudorandom (PR) sequences with binary values 0 and 1, and sequence lengths are sufficient to analyse the effect of intersymbol interference (ISI) from PMD. Currently, non-return to zero (NRZ), return to zero (RZ), and Manchester are the commonly used schemes in lightwave communications. NRZ codes are simple and easy to implement, so they are adopted in this simulation. In the system considered, a raised cosine filter [31] is used to shape the optical pulse at the transmitter. The transmitted waveform in the electrical domain is of the form

$$s(t) = \sum_{k=1}^{N} a_n h_t(t - kT), \qquad (2.1)$$

where a_n is the PR data stream, having the properties of being zero mean, unit variance, and mutually uncorrelated in time; the symbol rate is $1/T$ and N is the length of the PR sequence. $h_t(\cdot)$ is a bandlimited raised cosine pulse and defined to be

$$h_t(t) = \left(\text{sinc}(2Wt)\right)\left(\frac{\cos(2\pi Wt)}{1 - 16\alpha^2 W^2 t^2}\right), \qquad (2.2)$$

where parameter α is called the rolloff factor, $0 \le \alpha \le 1$, and it indicates the excess bandwidth over the minimum bandwidth W in Hz; $\alpha=0$ indicates no excess bandwidth.

To simulate a 10 Gb/s optical communication system, the parameters are given as follows:

$\alpha=1$ rolloff factor,

$c=2.998\times10^8$ m/s   light velocity,

B=10 Gb/s   bit rate, and

W=5 GHz   minimum bandwidth.

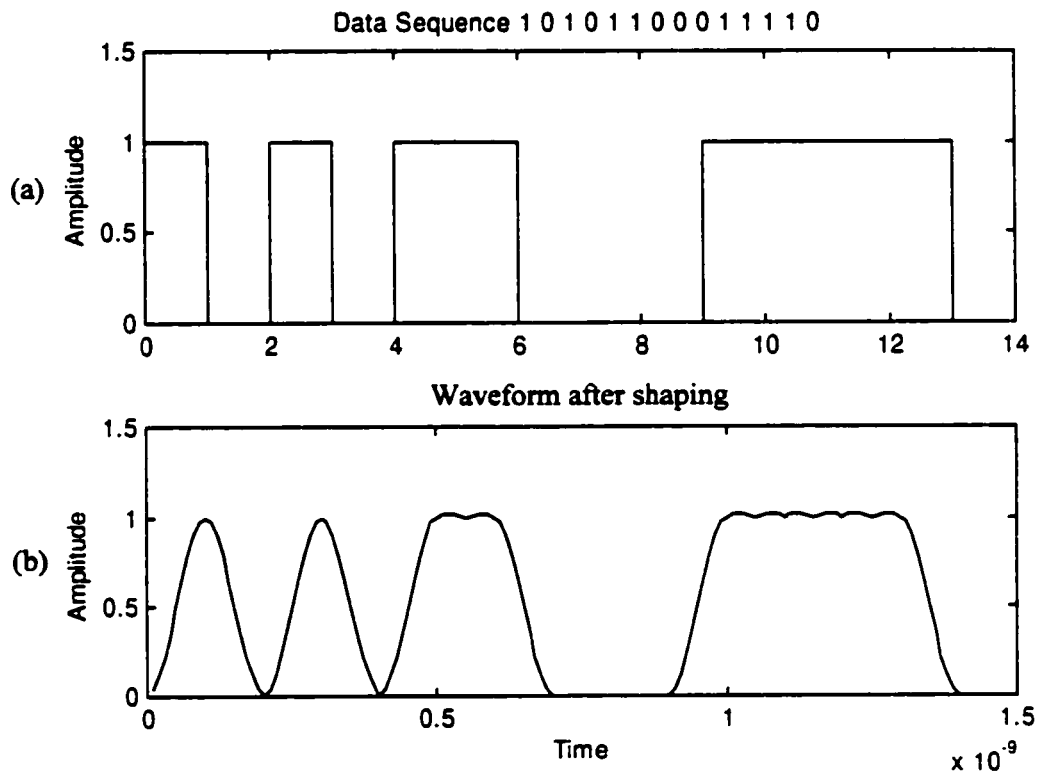The baseband electrical signal amplitude at the transmitter should be greater than

Figure 2.2 Data Generator Output Waveform Simulation

or equal to zero for the optical system. Fig. 2.2 shows the simulated value of the data

generator output. The upper diagram shows the NRZ sequence 1010110001110; the

lower diagram is this sequence after the transmitter pulse shape filter $h_t(t)$ [16].

2.2 Channel

The channel can be simulated by utilizing ensemble models of PMD. In a single-mode fiber, an optical wave of arbitrary polarization can be represented as the linear superposition of two orthogonally polarized HE_{11} modes [1]. In ideal fiber, the two HE_{11} modes are indistinguishable (degenerate) in terms of their propagation properties owing to the cylindrical symmetry of the waveguide. Real fiber, contain some amount of anisotropy owing to accidental loss of circular symmetry. This loss occurs either through a noncircular waveguide geometry or a nonsymmetrical stress field in the glass. In either case, the loss of circular symmetry gives rise to two distinct HE_{11} polarization modes with distinct phase and group velocities. All polarization effects in single-mode fiber are a direct consequence of this accidental loss of degeneracy for the polarization modes [1].

When subjected to a uniform perturbation in a short section of fiber, a single mode fiber becomes bimodal owing to a loss of degeneracy for the two HE_{11} modes. This can be expressed as a difference in the local propagation constants for the modes (β_s, β_f),

$$\beta_s - \beta_f = \frac{\omega}{c}(n_s - n_f), \qquad (2.3)$$

where β_s and β_f are propagation constants for the slow and fast modes; ω is the angular frequency of the light, c is the speed of light in vacuum, and n_s and n_f are the effective indices of refraction for the slow and fast modes respectively. The differential phase velocity indicated by Eq. (2.3) is usually accompanied by a difference in the local group velocities for the two modes which can limit the bandwidth of a fiber by broadening the pulse.

Fortunately, polarization effects do not accumulate in long fiber spans in a linear

fashion. Instead, because of random variations in the perturbations along a fiber span and

the mode coupling, the effects of one section of a fiber span may either add to or subtract

from the effects of another section. As a result, PMD in long fiber spans accumulates in a

random-walk-like process that leads to a square root of length dependence [9]. Fig. 2.3 is

Intrinsic Fiber Birefringence

+

Random Polarization Mode Coupling

+

Birefringent Components in Transmission Line
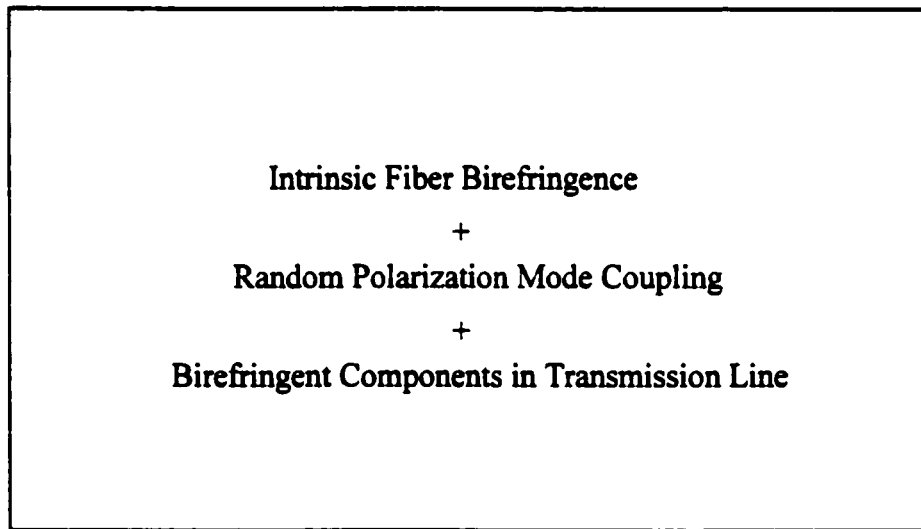
Figure 2.3 Origins of Polarization Mode Dispersion

a summary of origins of polarization mode dispersion.

The end-to-end system including the modulators and the demodulators is shown in

Fig. 2.4. It is convenient to view this linear system as a two-input port two-output port

optical network and characterize it by a 2×2 matrix impulse response or its matrix Fourier

transform, which is the overall system frequency response (see chapter 3). $h_{11}(t)$ and

$h_{22}(t)$ represent the co-polarized impulse responses, while $h_{12}(t)$ and $h_{21}(t)$ represent the

cross-polarized impulse responses due to mode coupling [11].
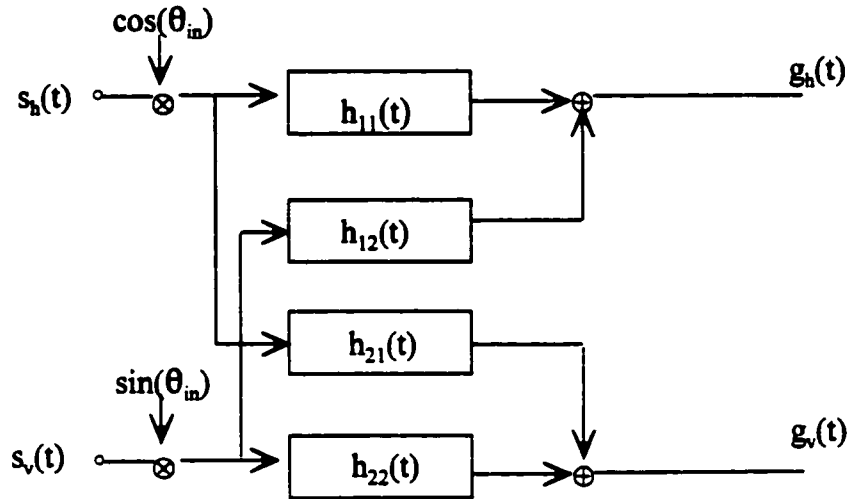
Figure 2.4 Channel model

The input is decomposed as two synchronous data signals: $s_v(t)$ and $s_h(t)$ which denote

vertical and horizontal channels. These are given as (see Fig. 2.4)

$$s_h(t) = \sum_{k=1}^{N} a_n h_t(t - kT)\cos(\theta_{in}),$$

$$s_v(t) = \sum_{k=1}^{N} a_n h_t(t - kT)\sin(\theta_{in}),$$

(2.4)

where θ_{in} is the angle between input pulse and horizontal channel describing the input

direction of the linear input polarization. $h_t(t-kT)$ was described in section 2.1.

It is now easy to verify that the relationship between the input and output can be

expressed as follows

$$g_h(t) = s_v(t) * h_{12}(t) + s_h(t) * h_{11}(t),$$

$$g_v(t) = s_v(t) * h_{22}(t) + s_h(t) * h_{21}(t), \tag{2.5}$$

where * denotes convolution. $g_v(t)$ and $g_h(t)$ denote the received horizontal and vertical optical signal at the receiver. In a compact form, it can be written as

$$g(t) = h(t) * s(t) = \int_{-\infty}^{+\infty} h(t - \tau)s(\tau)d\tau, \tag{2.6}$$

where the vector

$$s(t) = \begin{bmatrix} s_h(t) \\ s_v(t) \end{bmatrix}, \tag{2.7}$$

is the input optical signal vector and the vector

$$g(t) = \begin{bmatrix} g_h(t) \\ g_v(t) \end{bmatrix}, \tag{2.8}$$

is the received optical signal. $h(t)$ is the 2×2 matrix optical channel impulse response and is given by

$$h(t) = \begin{bmatrix} h_{11}(t) & h_{12}(t) \\ h_{21}(t) & h_{22}(t) \end{bmatrix}, \tag{2.9}$$

and the * between the matrix $h(t)$ and the vector $s(t)$ denotes matrix convolution.

To accommodate coupling between the polarized channels, one pair of impulse

responses ($h_{11}(t)$, $h_{22}(t)$) associated with the co-channel and the other pair ($h_{12}(t)$, $h_{21}(t)$) associated with the cross-channel, are used to completely characterize the PMD fiber medium.

2.3 Receiver

In a lightwave system, the electronics following the photodetector first amplify and shape the incoming signal and apply it to a decision circuit. The signal is also disturbed by thermal noise and shot noise due to the preamplifier, postamplifier, and timing circuits. The simulation discussed here accounts for the shaping of the received signal and the added thermal noise. The receiver is modeled as a filter with additive Gaussian noise at the input. The baseband filter is a second-order Butterworth filter with a 3-dB bandwidth equal to 0.65 times the modulation rate (Fig. 2.5). The receiver degradation depends on the relative power coupled into the polarization states, and the worst case degradation occurs when the two PSPs have equal power. It is well known that shot noise and thermal noise are the two fundamental noise mechanisms responsible for current fluctuations in all optical receivers even if the incident optical power P_{in} is constant. With direct detection, noise in the electrical signal is primarily due to thermal noise in the receiver because of the limitation of the detectors. With coherent detection, the shot noise is due to both the received and local oscillator signals. If the local oscillator is strong enough, the shot noise dominates the thermal noise. The thermal noise variance σ_T^2 becomes

$$\sigma_T^2 = (\frac{4k_BT_a}{R_L})\Delta f \tag{2.10}$$

and the variance of the shot noise σ_s^2 is given by

$$\sigma_s^2 = 2q(I_p + I_d)\Delta f, \qquad (2.11)$$

where Δf is the effective noise bandwidth; q is the electron charge. k_B is the Boltzmann's

constant, T_a is the absolute temperature, and R_L is the load resistor. I_p and I_d are the

current from the received optical signal and the dark current respectively [17]. It is well

known that the high intensity shot noise can be modeled as additive Gaussian noise [26].

Consequently, we do not need to consider the received optical signal from a quantum

physics point of view. Thus, for simplicity we will assume that the noise v(t) in the

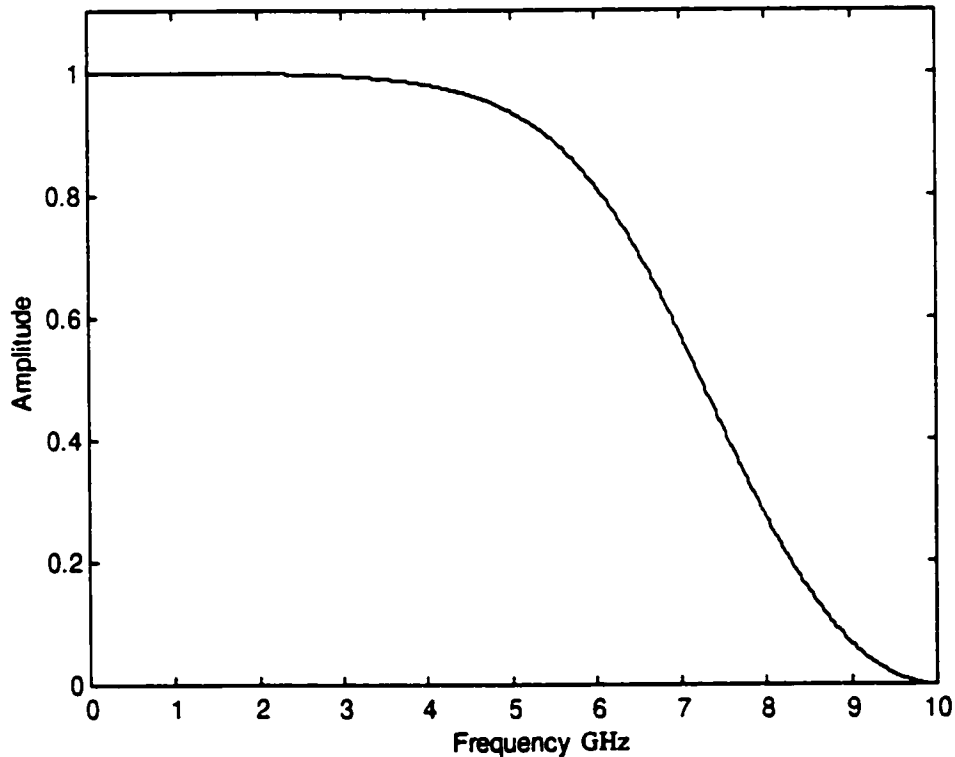electrical signal is additive Gaussian-distributed white noise.

Figure 2.5 Magnitude Response of the Butterworth Filter

The block diagram in Fig. 2.1 does not show details of the receiver. Fig. 2.6

shows the detail including the optical transversal filter used to compensate for ISI. The

optical transversal filter will be described in section 2.4, and channel estimation will be

discussed in chapter 4.
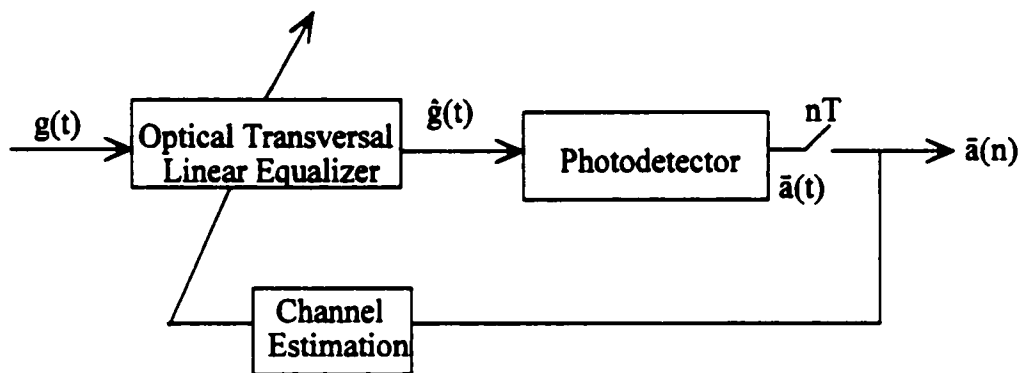
Figure 2.6 Optical Transversal Linear Equalizer Receiver

The input to the receiver is the signal g(t) which enters the linear optical

equalizer's filter. This filter has an impulse response $h_r(t)$, and the output of the filter is

the optical signal ĝ(t) which satisfies:

$$\hat{g}(t) = g(t) * h_r(t) .$$
(2.12)

At the receiver, the noise is proportional to the receiver bandwidth and can be reduced by

using a low pass Butterworth filter. The optical equalizer is used to compensate ISI from

PMD. The received electrical signal ā(t) after the photodetector (from Eq. 2.14) is then

fed to the sampler, which operates at the symbol rate, 1/T. The output of sampler is the

signal ā[n].

2.4 Optical Transversal Filter

Optical signal processing is expected to effectively handle high-speed broadband signals in advanced optical point-to-point communication systems and networks. In particular, optical signal processing using waveguides as a delay medium has the advantage of being able to process broadband signals because of the large available bandwidth of optical waveguides [6].

Optical transversal filters using coherent interference can express arbitrary tap weighting coefficients and can process signals without inherent combining loss. This filter can process optical signals without converting them into electrical signals. The filter therefore has a theoretical operating bandwidth of up to half of the optical carrier frequency. However, the actual filter has a bandwidth limitation due to the operating bandwidth limit of its optical components, especially the directional coupler.

Transversal filters have three essential functions: delay, multiplication, and summation. A coherent optical transversal filter block diagram is shown in Fig 2.7. Using tunable optical power splitters and phase shifters, arbitrary complex tap coefficients can be expressed by electrically controlled amplitude and carrier phase. The light phase in each tap is shifted either 0 or π, thus it can synthesize negative tap coefficients optically. At the output of the filter, these split signals are coherently combined. Various transfer functions of the transversal filter can be obtained appropriately by controlling the tunable splitter and phase shifter. The number of taps m

and unit delay time τ determine the resolution in the frequency domain. The greater m,
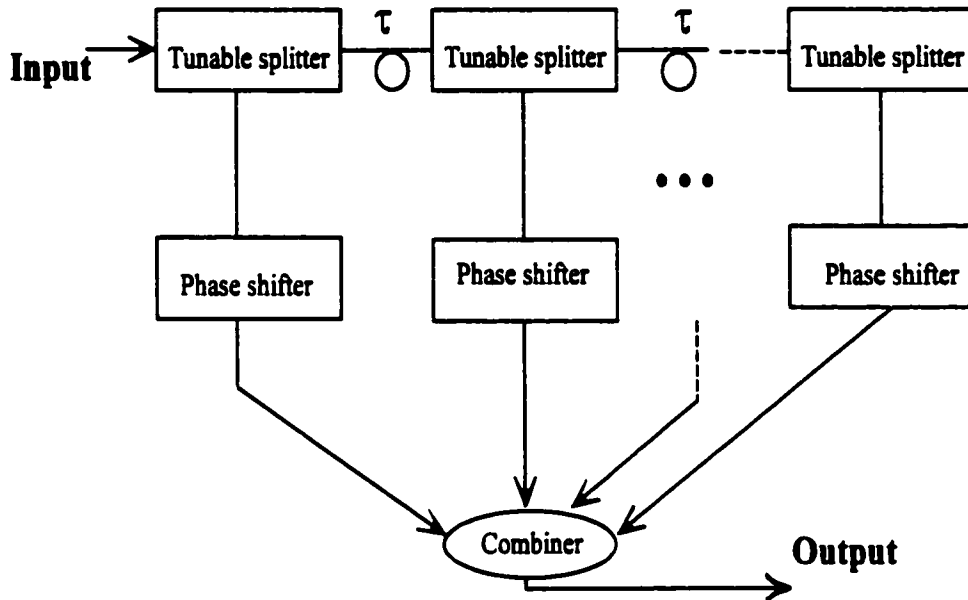
Figure 2.7 Configuration of The Coherent Optical Transversal Filter

the more detailed the frequency characteristics, the shorter τ , the higher the time-domain

resolution in processing the input waveform. For the symbol-spaced equalizer, τ is100

ps. For the fractionally spaced equalizer, the tap spacing is T/2, which is 50 ps.

The theoretical impulse response of the transversal filter in the time domain is

$$h_r(t) = \sum_{k=1}^{m} w(k) e^{jp(k)} \delta(t - k\tau). \qquad (2.13)$$

where w(k) is the splitting ratio of the k-th splitter, p(k) is the phase shift of the k-th

phase shifter, which is either 0 or π. $\delta(t)$ is the Dirac delta function, m is the number of

taps and τ is the unit delay time [24]. The frequency response is obtained by taking the

Fourier transform of $h_r(t)$ from Eq. 2.13.

By definition, the Fourier transform of the signal $h_r(t)$ is given by the integral

$$H_r(f) = \int_{-\infty}^{+\infty} h_r(t)e^{-j2\pi ft} dt .$$

(2.14)

The impulse response of the transversal filter has a periodicity which corresponds

to the inverse of the time delay τ. w(k) can be obtained from channel estimation (see

chapter 4).

In real time, the tunable splitters can be programmable optical couplers, or erbium

doped fiber amplifiers (EDFA) [45], or Mach-Zehnder modulators [17] to change the

weight of the optical filter taps. The phase shifter may be a $LiNbO_3$-based phase

modulator which is used to get a bipolar impulse response [17]. The optical transversal

filter is different from a traditional electrical filter due to its large bandwidth. It should be

operated adaptively via a microprocessor to compensate for the time varying PMD.

Chapter 3

Polarization Mode Dispersion

This chapter will present, in detail, the mathematical description of the PMD model. This model based on principal states was first introduced by C.D. Poole [3]. The distortion caused by PMD is demonstrated in the form of eye diagrams. Understanding PMD is fundamental in order to compensate for it.

3.1 PMD Waveplate Model

For each frequency ω, it has been shown that there exists a pair of orthogonal input and corresponding output states of polarization, referred to as principal states polarization. Signals transmitted in either of these two states have no first-order PMD, but the two states have, in general, different time delays. Thus, a signal transmitted with arbitrary polarization can be described using these PSPs as basis functions [3]. A single-mode optical fiber with PMD can be modeled by a 2×2 complex transfer matrix $h(\omega)$, which, assuming no polarization-dependent loss, is given by

$$h(\omega) = e^{\beta(\omega)}U(\omega) = e^{\beta(\omega)}\begin{bmatrix} u_1(\omega) & u_2(\omega) \\ -u_2^*(\omega) & u_1^*(\omega) \end{bmatrix}, \tag{3.1}$$

where ω is the optical frequency, $U(\omega)$ is a unitary Jones matrix; $u_1(\omega)$ and $u_2(\omega)$ are elements of the Jones transfer matrix and $\beta(\omega)$ is determined by the polarization-

independent phase shift and loss of the fiber given by

$$\beta(\omega) = -z[\rho + j\psi(\omega)] , \qquad (3.2)$$

where z is the transmission distance, ρ represents the fiber loss and $\psi(\omega)$ is the

propagation constant; the superscript * denotes complex conjugate, and

$|u_1(\omega)|^2 + |u_2(\omega)|^2 = 1$, for all ω. The difference in arrival times, is defined as

$$\Delta\tau = 2\sqrt{|u_1'|^2 + |u_2'|^2} . \qquad (3.3)$$

where the primes denote differentiation with respect to angular frequency.

Thus, the output optical field $\overline{E_b}$ with a monochromatic optical input field $\overline{E_a}$ is

given by

$$\overline{E_b} = h(\omega)\overline{E_a} . \qquad (3.4)$$

Thus, provided the source spectrum satisfies the narrow band assumption, the time

varying output electrical field vector $\overline{E_b}$ of a long fiber will have the general form [1]:

$$\overline{E_b} = c_+\overline{\varepsilon}_+E_a(t + \tau_+) + c_-\overline{\varepsilon}_-E_a(t + \tau_-), \qquad (3.5)$$

where E_a is the electrical signal input to the transmit laser, c_- and c_- are the fraction of the

input signal into each of the PSPs, $\overline{\varepsilon}_+,\overline{\varepsilon}_-$ are unit vectors specifying the output

polarization states of the two components which are referred to as output principal states.

The difference of arrival time $\Delta\tau = \tau_- - \tau_+$ is the DGD, which gives rise to pulse

broadening at the output of a fiber when energy is split between the two principal states at

the input. In general, the amount of broadening depends on the power splitting ratio between the pulses determined by the coefficients c_+ and c_-, as well as the difference in the delays, $\Delta\tau$. Both the PSPs and DGD are assumed to be independent of frequency if only first-order PMD is being considered.

An immediate consequence of the property of polarization invariance with frequency is that an optical pulse that is aligned with a principal state at the input of a fiber will emerge at the output with its spectral components all having the same state of polarization. This in turn implies that the only distortion on the pulse that can occur is a pure phase distortion, which, to first order, does not change the shape of the pulse but only shifts it in time. Thus, an optical pulse that is aligned with a principal state at the input of a fiber thus emerges both polarized and unchanged in shape to first order.

To numerically compute the statistics of both first- and second-order PMD, we simulate a real single-mode fiber by randomly concatenating a sequences of segments, each with different random PSPs (see Fig. 3.1) [23, 33]. Applying this model, the output pulse at the end of the fiber is obtained by successively multiplying the single segment matrices, each with different (random) PSPs, but with fixed delays of

$$\tau_k = \frac{\langle\Delta\tau\rangle}{\sqrt{K}}, \qquad\qquad k=1,2,3,\dots,K \qquad\qquad (3.6)$$

where τ_k is the DGD introduced by the k-th segment of the fiber and K is the number of segments. $\Delta\tau$ is the mean DGD value.

The overall transfer matrix is then

$$U(\omega) = \prod_{k=1}^{K} M_k(\omega) , \qquad (3.7)$$

where $M_k(\omega)$ is k-th transfer matrix [51] given by

$$M_k(\omega) = \begin{bmatrix} \cos(\varphi_k) & \sin(\varphi_k) \\ -\sin(\varphi_k) & \cos(\varphi_k) \end{bmatrix} \begin{bmatrix} e^{\frac{j\omega\tau_k}{2}} & 0 \\ 0 & e^{-\frac{j\omega\tau_k}{2}} \end{bmatrix}, \qquad (3.8)$$

where $\{\varphi_k, k=1,2,3,...,K\}$ are a set of independent identically distributed random variables denoting random polarization and phase of the k-th segment. Their probability density functions are

$$P(\varphi_k) = \begin{cases} \dfrac{1}{2\pi} & -\pi < \varphi_k \leq \pi, \\ 0 & \text{otherwise}. \end{cases} \qquad (3.9)$$

Figure 3.1 Modeling PMD in Single Mode Fiber
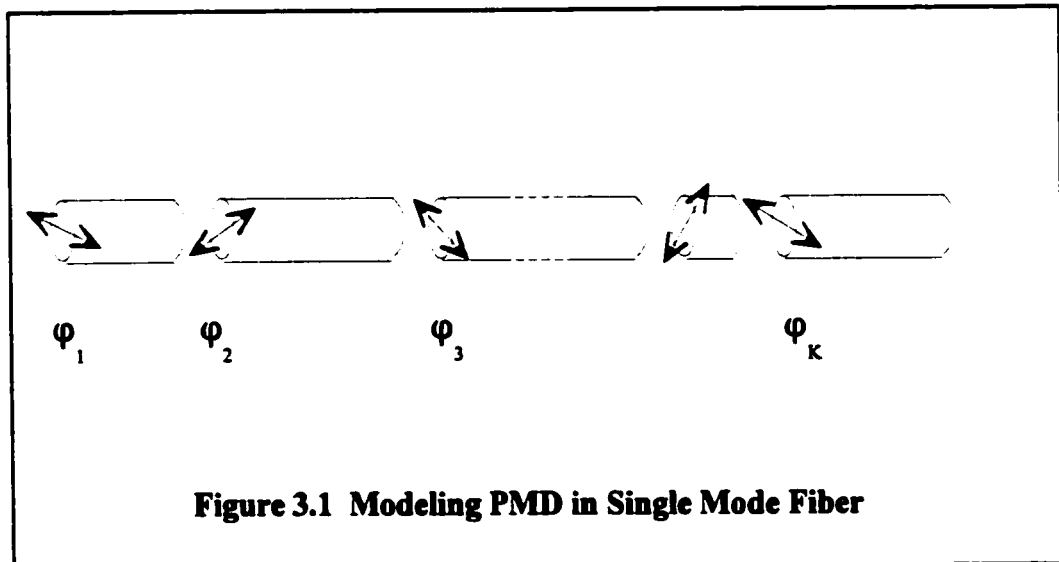
The received signal in the time domain is given by

$$h(t) = F^{-1}\{h(\omega - \omega_c)\} , \qquad (3.10)$$

where ω_c is the angular carrier frequency, and F^{-1} denotes the inverse Fourier transform. The inverse Fourier transform is defined as

$$h(t) = \int_{-\infty}^{+\infty} H(f)e^{j2\pi ft}df . \qquad (3.11)$$

Optical digital information bearing signals are transmitted by some type of carrier modulation. All the previous equations are based on a passband model. The channel over which the signal is transmitted is limited in bandwidth to an interval of frequencies centred about the carrier or adjacent to the carrier. The carrier frequency is on the order of 100 THz while the bandwidth of the channel is about a few GHz (OC-192). With no loss of generality and for mathematical convenience, it is desirable to reduce all passband signals and channels to equivalent baseband signals and channels. The term baseband is used to designate a band of frequencies representing the original signal as delivered by a source of information. The conversion from passband signal to baseband signal is defined as

$$h_b(t) = (h(t)e^{-j2\pi f_c t})w_f(t) ,$$

$$H_b(f) = H(f + f_c)W_f(f), \qquad (3.12)$$

where $h_b(t)$ is the baseband impulse response, f_c is the optical carrier frequency [48,47], $w_f(t)$ is the impulse response of the low pass filter that is used to pass the frequency

components at 0, but to filter out the high frequency components at f_c and beyond. $W_f(f)$

is the Fourier transform of $w_f(t)$ and the one-sided bandwidth of $W_f(f)$ is B_f.

To sum up, the procedures to obtain the impulse response of optical channel with

PMD channel is as follows:

1. Select the average DGD, $<\Delta\tau>$.

2. Generate $\varphi_1, \varphi_2,...,\varphi_K$ which are uniformly distributed between $[0, 2\pi)$.

3. Calculate $\tau_1, \tau_2, \tau_3 ... \tau_K$ by Eq. 3.6, note $\tau_1 = \tau_2 = \tau_3 = ... = \tau_K$, K is the number of the

   segments.

4. Pick ω_1.

5. Calculate $M_1(\omega_1), M_2(\omega_1), M_3(\omega_1), ... , M_K(\omega_1)$.

6. Calculate $h(\omega_1)$.

7. Repeat 4), 5), 6), for $\omega_1, \omega_2...,\omega_k... , \omega_M$. Where ω_k is the k-th sample frequency and

   let M denote the number of frequency samples contained in frequency interval of B_f.

8. Convert signals and channels from passband to baseband to obtain $h_b(t)$.

The baseband impulse response of the optical channel with PMD (DGD=45 ps,

$\gamma=0.41$) is shown in Fig. 3.2 after taking the inverse Fourier transform. In this case, $h_{11}(t)$

and $h_{22}(t)$ represent horizontal and vertical channel respectively, while $h_{12}(t)$ and $h_{21}(t)$

represent the coupling between the horizontal and vertical channel, which indicates the

channel is depolarized. If there is no PMD, the impulse response of $h_{12}(t)$ and $h_{21}(t)$

should equal 0, which means there is no cross polarization.

For a fiber much longer than the characteristic length of the mode coupling, the

DGD is known to have a Maxwellian probability density function (PDF) in the form [42],

$$PDF(\Delta\tau) = 3\sqrt{\frac{6}{\pi}} \frac{\Delta\tau^2}{\Delta\tau_{rms}^3} \exp(-\frac{3\Delta\tau^2}{2\Delta\tau_{rms}^2}),$$ (3.13)

where $\Delta\tau_{rms}$ is the quadratic mean value of $\Delta\tau$ ($\Delta\tau_{rms} = \langle \Delta\tau^2 \rangle^{1/2}$) and has a square root

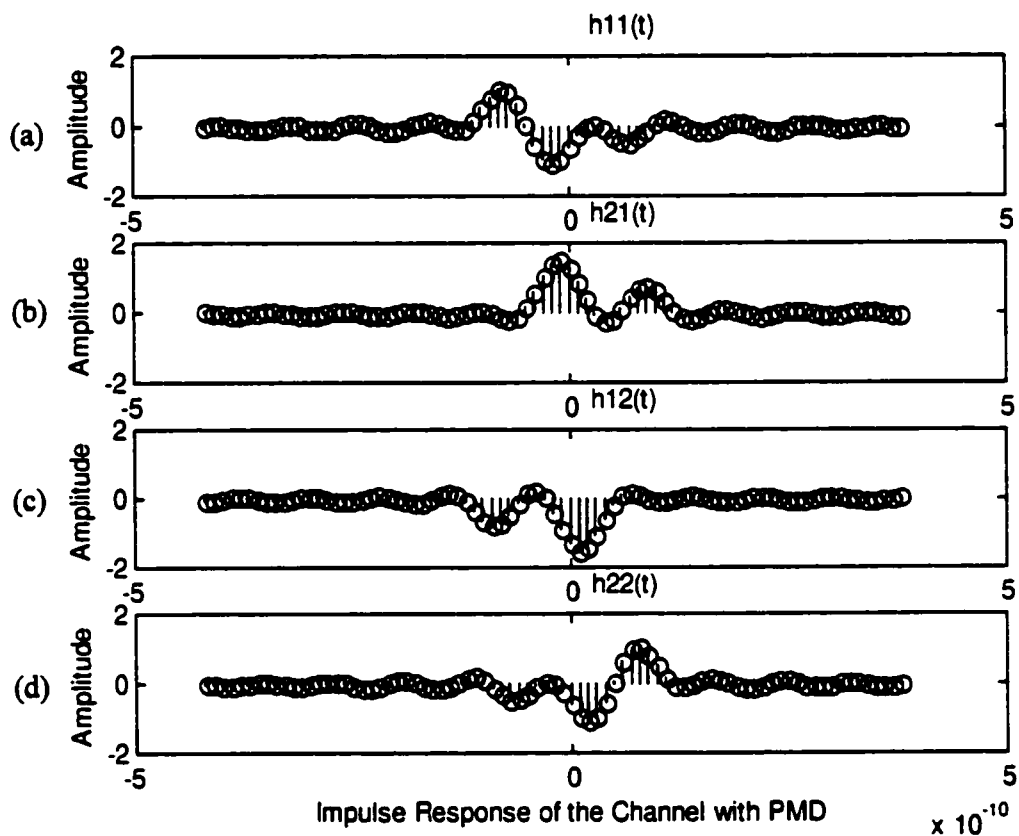dependency with length [1].

Figure 3.2 Impulse Response of Channel With PMD

In high-bit rate systems, because of the sensitivity to the environment, PMD can

lead to fading of the baseband signal in many ways analogous to multipath fading in radio

systems. Such fading would affect both coherent and direct detection systems [4]. A

time-varying model for PMD is given using a model based on Brownian motion [46],

which is not included in this thesis.
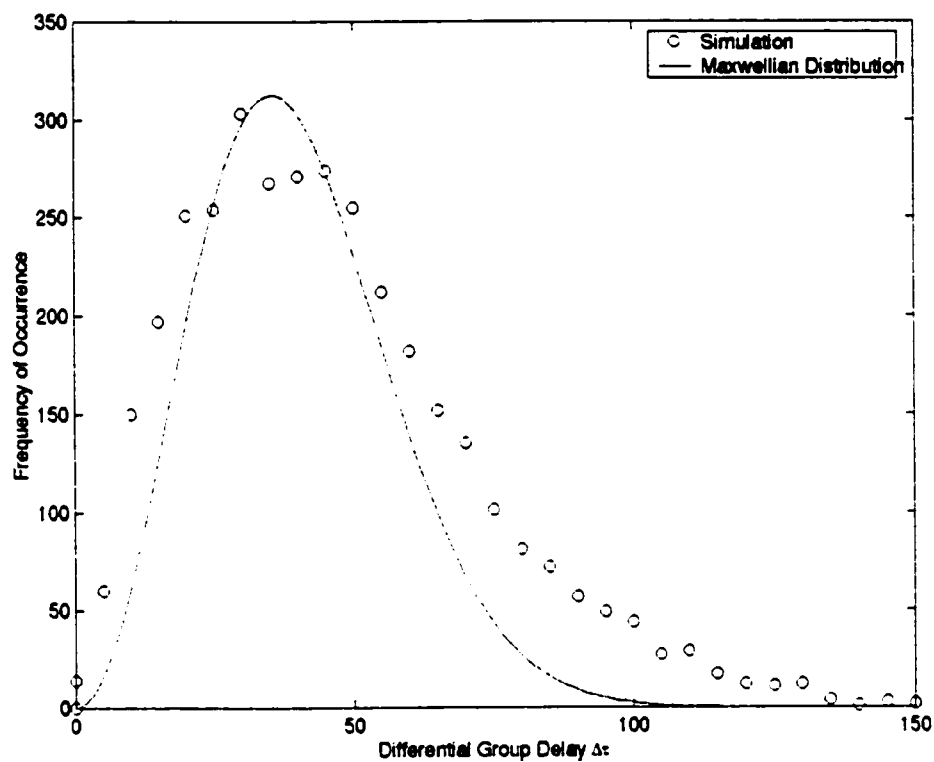
Figure 3.3 Numerical Simulation of First Order PMD in an Optical Fiber

Fig. 3.3 compares the Maxwellian probability density function of PMD with the

numerical simulation measured data DGD by randomly changing the coupling parameters

φ_k. The points from the simulation differ from the theoretical values because of the

limited number of statistically independent samples. The simulations had 3500 samples

with 150 randomly coupled sections.

3.2 PMD Induced Distortions

Digital lightwave systems rely on undistorted transmission of an optical pulse through long lengths of fiber. Dispersive effects such as PMD cause pulse spreading and distortion and thus can lead to system penalties [29,10].

Experiments show PMD induced variations in bit error rate performance are subjected to ambient temperature changes in a field environment [52]. The correlation between rapid fluctuations in bit error rate and steep changes in ambient temperature during sunrise and sunset illustrates how performance variations related to PMD can be directly tied to environmental conditions. A system designed with adequate margins for normal conditions may have unacceptable penalties under rare conditions of extremely high PMD [1].

Therefore PMD is a time-varying, stochastic effect and the system penalties are also time varying. Thus, the equalizer should be adaptive.

In this section, the pulse shape is analysed by computing the mean transmit time and root mean square (RMS) of the output pulse. Since the previous analysis has revealed that the various degradations due to first-order PMD induce splitting and broadening, we expect the system penalties to be closely related to the variations of the mean transmit time and RMS pulse width [2].

We define the mean transmit time and the RMS width of the output pulse by

$$\langle \eta \rangle = \frac{\int_{-\infty}^{+\infty} \eta P_{out}(\eta)d\eta}{\int_{-\infty}^{+\infty} P_{out}(\eta)d\eta} \quad , \tag{3.14}$$

which is the normalized mean transit time and

$$RMS^2 = \frac{\int_{-\infty}^{\infty} \eta^2 P_{out}(\eta)d\eta}{\int_{-\infty}^{\infty} P_{out}(\eta)d\eta} - \langle \eta \rangle^2 , \tag{3.15}$$

which is the normalized RMS width; the pulse power at the receiver output can be

computed from

$$P_{out}(\eta) = |\bar{a}(\eta)|^2 , \tag{3.16}$$

where $\bar{a}(\eta)$ is the received electrical signal. The shortest mean transmit time means the

SOP of the input signals is aligned with the fast PSP at the central frequency [13]. Thus

PSPs can be obtained by varying the input SOP and searching for the maximum relative

delay between the two output sequences, with the minimum distortions on the isolated

"1" bits [15].

A useful tool to evaluate the combined effect of impairments on the overall system

performance is the so called eye pattern [31] which is defined as the synchronized

superposition of all possible realizations of the signal of interest viewed within a particular interval. The interior region of the eye pattern is called the eye opening. An eye pattern provides a great deal of useful information about the performance of a data transmission system such as the sensitivity of the system to timing error and the noise margin. When the effect of intersymbol interference is severe, traces from the upper portion of the eye pattern cross traces from the lower portion, with the result that the eye is completely closed. In such a situation, it is impossible to avoid errors due to the combined presence of intersymbol interference from PMD and noise in the receiver.

The performance criterion considered is the optical signal power penalty due to interference, which is the increased optical signal power required to maintain the same eye opening with intersymbol interference. The optical signal power penalty can be derived from the minimum eye opening over all input bit sequences. The minimum eye opening is the minimum sampled signal values for a "1" minus the maximum sampled signal value for a "0", with no noise at the receiver. Thus, if the difference between the signal levels for a "1" and a "0" without ISI is Y, the eye opening relative to the maximum eye opening is denoted by *eye* and is given by

$$ eye = \frac{\min(\text{eye opening})}{Y} . \tag{3.17} $$

The optical power penalty is given by [26]

$$ penalty = 10\log_{10}(eye) \qquad \text{for direct detection, and} $$

$$ penalty = 20\log_{10}(eye) \qquad \text{for coherent detection,} \tag{3.18} $$

since the received current is proportional to the optical power with direct detection and

the received current is proportional to the magnitude of the optical field with coherent

detection.

The eye patterns in Fig 3.4 demonstrate the impact of the DGD distortion. From

Fig. 3.4(a) and Fig. 3.4(b) it is clear that the pulse transmitted from one of the PSPs has

the minimum distortion and the eye is open widely, even when the DGD is 96 percent of

a symbol period. However, a pulse received in the worst polarization, shown in Fig. 3.4

(c), has a closed eye. It agrees well with the theory provided by C.D.Poole [3]. Thus
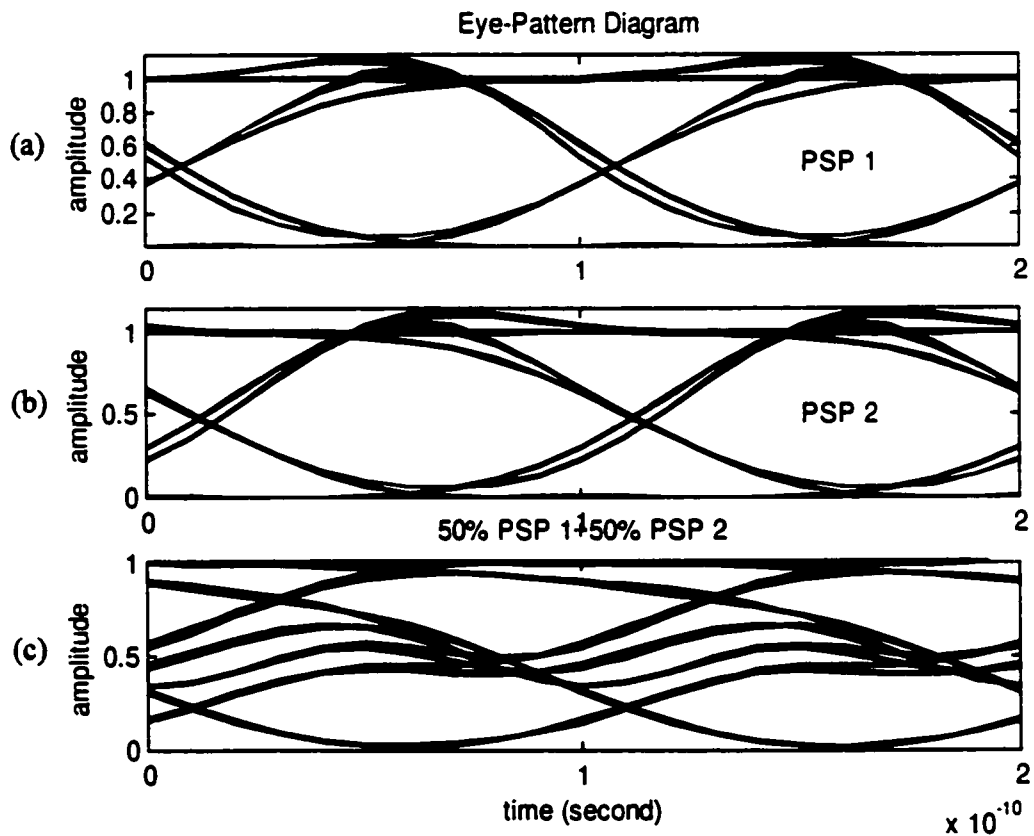

Figure 3.4 Simulated Eye Diagram of 10 Gb/s Signal Transmitted in Principal States of Polarization (PSP) with 96 ps DGD

some people have used this idea to compensate for PMD by adjusting the input to one of its PSPs [51]. The interference is so severe that the eye is almost closed when the input power splitting ratio between the fast PSP and slow PSP is 0.5, which is the worst case (see Fig. 3.4(c)).

Fig. 3.5 shows the distortion induced by various DGDs for the worst case of power splitting, $\gamma=0.5$. These DGDs are 0 ps, 58 ps and 92 ps, respectively. The power penalty for 58 ps of DGD is 2.21 dB (from Eq. 3.18), while the power penalty is 9.2 dB when the DGD is 92 ps. In these two cases, the power penalty is much more than 1 dB to be accepted by the system. Thus, ISI from PMD should be reduced. Some methods will be discussed in chapter 4.
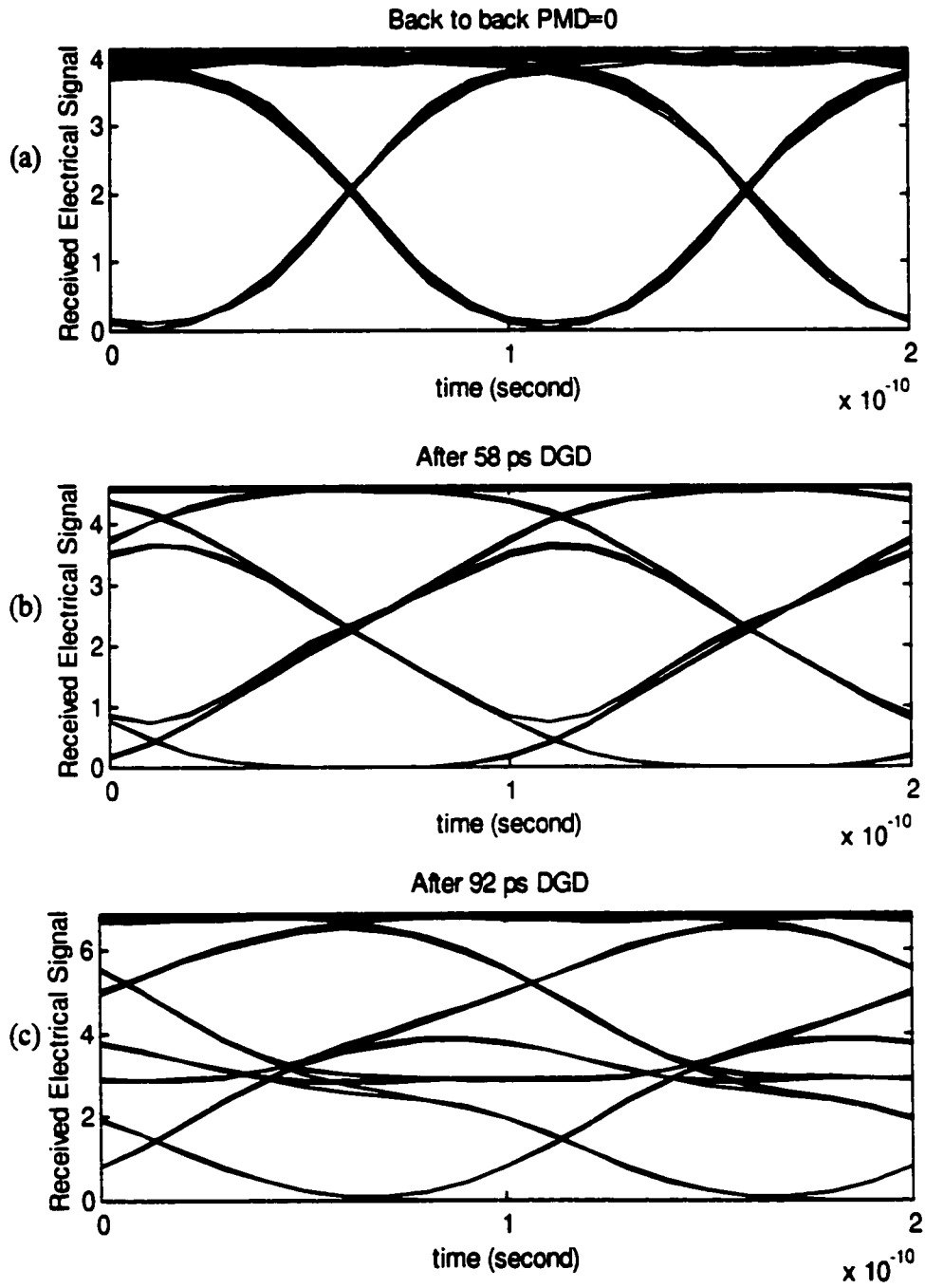
**Figure 3.5 Simulations of PMD -Induced Pulse Distortions in a
10 Gb/s for Various DGD Values (Worst Case γ=0.5)**

Chapter 4

Channel Estimation by Correlation

This chapter will discuss a technique for channel identification. A channel

estimation algorithm is presented for estimating a channel impulse response from a

known training sequence whose power is much lower than that of the information-bearing

signal, and these two signals are added together at the transmitter. The performance of

the technique is also investigated.

4.1 Adaptive Equalization

In digital optical communications a considerable effort has been devoted to the

study of data transmission systems that utilize the available channel bandwidth

efficiently. The objective is to design a system that accommodates the highest possible

rate of data transmission, subject to a specified reliability that is usually measured in

terms of the bit error rate or eye pattern. The transmission of digital data through a linear

optical communication channel is limited by two factors [46], intersymbol interference

(ISI) and noise. ISI is caused by distortion such as chromatic dispersion and polarization

mode dispersion. Chromatic dispersion is not discussed in this thesis. Noise is generated

by the receiver in its front end. Thermal noise and shot noise in the receiver are

considered as Gaussian noise in this thesis.

For bandwidth limited channels, ISI is the chief determining factor in the design of

high data rate optical transmission systems.

To overcome the intersymbol interference problem, control of the time sampled received signal is required. In principle, if the characteristics of the transmission medium are known precisely, then it is virtually always possible to design a pair of transmit and receive filters that will make the effect of ISI (at sample times) arbitrarily small. This is achieved by proper shaping of the overall response of the channel in accordance with Nyquist's classic work. In practice the channel ISI from PMD is time varying, due to variations in the transmission media and temperature, which makes the received signal nonstationary. Accordingly, the use of a fixed pair of transmit and receive filters, designed on the basis of an average channel characteristic, may not adequately reduce ISI. This suggests the need for an adaptive equalizer that provides precise control over the time response of the channel.

A device well-suited for the design of an adaptive filter is depicted in Fig. 4.1. The impulse response of the adaptive filter is

$$h_r(t) = \sum_{k=1}^{m} w_k \delta(t - kT) \,, \tag{4.1}$$

where $\delta(t)$ is the Dirac delta function; w_k is the k-th tap weight and the delay T is chosen equal to the symbol period.

Suppose that the adaptive filter is connected in cascade with a linear system whose impulse response with PMD is $h(t)$. Let $p(t)$ denote the impulse of the equalized system. Then $p(t)$ is equal to the convolution of $h(t)$ and $h_r(t)$, as shown by

$$p(kT) = \sum_{k=1}^{m} w_k h(t) * \delta(t - kT),$$

$$= \sum_{k=1}^{m} w_k h(t - kT).$$

(4.2)

Thus, for no intersymbol interference $p(kT)$ should satisfy

$$p(kT) = \begin{cases} 1 & k = 0, \\ 0 & k \neq 0. \end{cases}$$

(4.3)

The task of the thesis is to obtain the impulse response of the optical fiber channel with PMD by channel estimation, then calculate the coefficients of the equalizer filter to compensate for PMD.

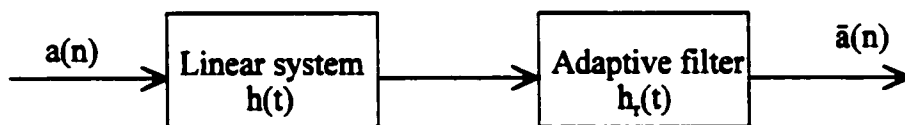Optical transversal filters (see section 2.4) can equalize any type of linear

Figure 4.1 Adaptive Filtering Scheme

distortion and can easily be made adaptive [27]. This chapter will discuss how to obtain

the impulse response of the PMD channel. Thus, the next question is how to calculate the

coefficients of the optical transversal filter. Calculating the coefficients will be discussed

in chapter 5.

4.2 Bandwidth Issues

The bandwidth of a signal provides a measure of the extent of significant spectral

content of the signal for positive frequencies. When the signal is strictly band limited, the

bandwidth is well defined. When, however, the signal is not strictly band limited, which

is generally the case, we encounter difficulty in defining the bandwidth of the signal. The

difficulty arises because the meaning of "significant", attached to the spectral content of

the signal, is mathematically imprecise. Although many mathematical definitions exist,

there is no universally accepted definition of bandwidth.

One definition of bandwidth is the null-to-null bandwidth, which is the width of

the main lobe for positive frequencies.

A popular definition of bandwidth is the 3-dB bandwidth. Specifically, if the

signal is low passed, the 3-dB bandwidth is defined as the separation between zero

frequency, where the amplitude spectrum attains its peak value, and the positive

frequency at which the amplitude spectrum drops to $1 / \sqrt{2}$ of its peak value.

In this thesis, we use "excess bandwidth" which indicates the bandwidth over the

ideal solution. In an OC-192 system, the ideal bandwidth is approximately 5 GHz. A

rolloff factor of 1 for the raised cosine pulse is used in this thesis meaning 100% excess

bandwidth. Specifically, the transmission bandwidth B_f is defined by

$$B_f = W(1 + \alpha),$$

(4.4)

where W is the minimum ideal bandwidth and α is the rolloff factor.

Fig. 4.2 shows the spectral content of the received electrical signals, with and

without PMD distortion. Comparing the spectrums of the received signal without PMD

and with PMD (DGD=78 ps, worst case γ=0.5), it indicates clearly some distortion from
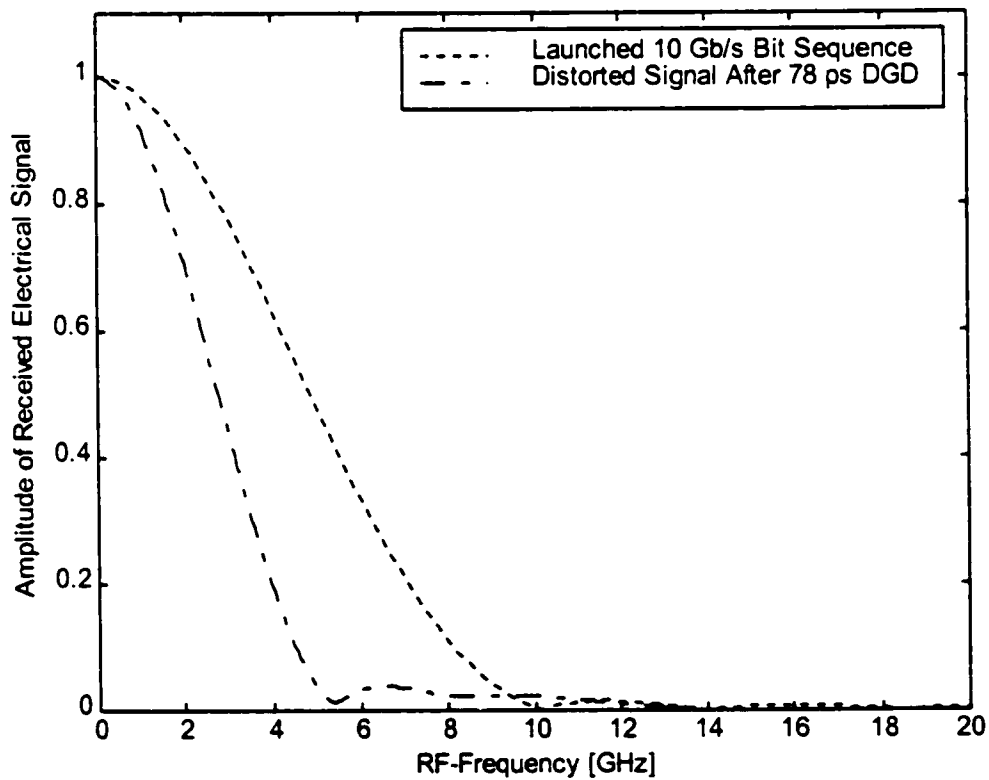

Figure 4.2   Simulation RF of Received Electrical Signal With
and Without PMD Distortion

PMD and it is the excess bandwidth that makes a fractional rate tap spacing equalizer necessary to compensate the distortion beyond 5 GHz.

4.3 Hardware Consideration

The PMD equalizer is realized with an optical tapped filter based on channel estimation (see Fig. 4.3). These are the steps:

❶. Add an optical training information signal d(n), also called a training sequence, with the optical information bearing signal a(n) at the transmitter, and let

$$10\log\frac{P1}{P2} = 30\,dB \quad , \tag{4.5}$$

where P2 is the power of the training information d(n) and P1 is the power of the optical information bearing signal a(n). P2 is 30 dB lower than P1 and does not affect the bit error rate (BER) at the receiver.

❷. Calculate the properties of the fiber by using correlation. The same training sequence, but time reversed, is used at the receiver in synchronism with the transmitter to correlate the received signal so that the channel response h(n) in the time domain may be obtained. The algorithm used in channel estimation is based on a minimum square error (MMSE) criterion [7]. This channel estimation is the critical part of this thesis.

❸. Set the coefficients of an optical filter to compensate for the fiber. Suppose the frequency response of the optical fiber channel is H(f), and the frequency response

of the optical equalizer is $H_r(f)$. To eliminate ISI from PMD completely, $H(f)H_r(f)$ should equal 1. After h(n) is obtained from the channel estimation, we can calculate the coefficients of the optical filter using deconvolution or an inverse filter. It must be noted that the optical filter must be adaptive to compensate for the time varying PMD.

❹. Every 0.2 ms (2×10^6 bits), we update the coefficients of the optical filter to make this scheme adaptive.

These functions, such as channel estimation by a training sequence and equalizer coefficient calculation are performed by microcomputer. Fig. 4.3 shows the proposed hardware implementation for this PMD compensation. There are two important issues to make sure this implementation is a success. One is the quality of the training signal, which means its autocorrelation should be similar to a delta function. The other is the power issue, since the training signal is much lower in power than the information bearing signal. A long sequence is needed to obtain an accurate estimate of the impulse response. With these two issues, the longer the sequence, the better the performance. In the ideal case, if the training sequence is infinite, we can get the exact the impulse response. But as mentioned before, the distortion caused by PMD is a time varying process and the time for it to change is on the order of several seconds [25]. We need to complete the equalizer calculation within this time. Thus, an extremely long training signal is not desirable. It is a tradeoff. We will consider these issues in the following sections.

Fig. 4.3 shows the required hardware implementation. The training sequence at

the receiver is the same, but time reversed, as the training sequence at the transmitter.

The optical filter is described in section 2.4, chapter 2, and it is used to compensate for

PMD. A computer is used to calculate the coefficients after sampling the incident optical
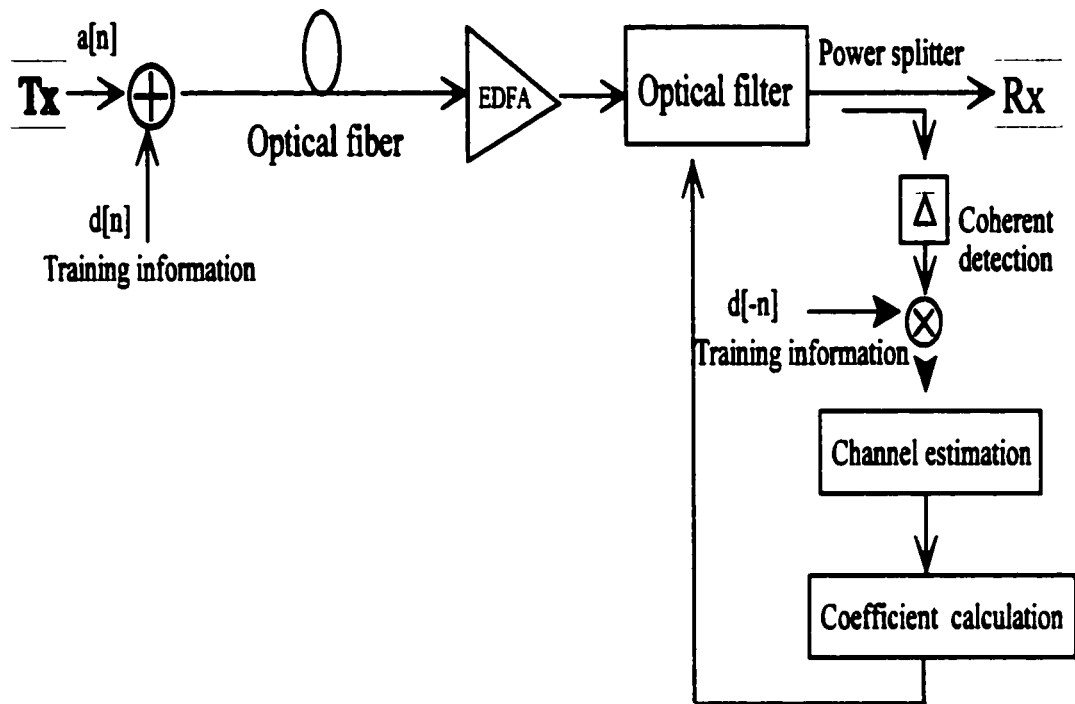
signal.

Figure 4.3 Channel Estimation Based on Coherent Detection

For the purpose of channel estimation, coherent detection is needed to keep the

phase information of the channel. Consider the electrical field associated with the

received optical signal and write it as [17, 50]

$$E_s = A_s \exp[-i(\omega_s t + \phi_s)], \qquad (4.6)$$

where ω_c is the carrier frequency, A_s is the amplitude, and ϕ_s is the phase. The optical field associated with the local oscillator is given by a similar expression

$$E_{LO} = A_{LO}\exp[-i(\omega_{LO}t + \phi_{LO})],\qquad(4.7)$$

where A_{LO}, ω_{LO}, and ϕ_{LO} are the amplitude, the frequency and the phase of the local oscillator, respectively. The received power at the photodetector is given by

$$P_{out} = k|E_s + E_{LO}|^2,\qquad(4.8)$$

where k is a constant. The photocurrent is given by

$$I(t) = 2RA_sA_{LO}\cos(\phi_s - \phi_{LO}),\qquad(4.9)$$

where R is the detector responsivity. Then, we get the important relationship

$$I(t) \propto A_s.\qquad(4.10)$$

This is the situation in direct detection where I(t) is proportional to A_s^2. With Eq. 4.10 we can see that in coherent detection I(t) is proportional to A_s, which is the amplitude of the optical signal distorted by PMD after transmission. Thus the phase information is preserved for use in channel estimation. This is the reason coherent detection is needed in channel identification.

4.4 System Identification from Correlation

Suppose there is a linear time-invariant system (see Fig.4.4), with known input d(t), unknown impulse response h(t), and output y(t), in this case, a matched filter d(-t) is not yet considered. d(t) is a noise like random process. The statistics of d(t) and y(t) are

known; y(t), h(t) and d(t) are related by the convolution integral [37]

$$y(t) = \int_{-\infty}^{+\infty} h(u)d(t-u)du,$$

or $\qquad y(t+\tau) = \int_{-\infty}^{+\infty} h(u)d((t+\tau)-u)du.$ $\qquad$ (4.11)
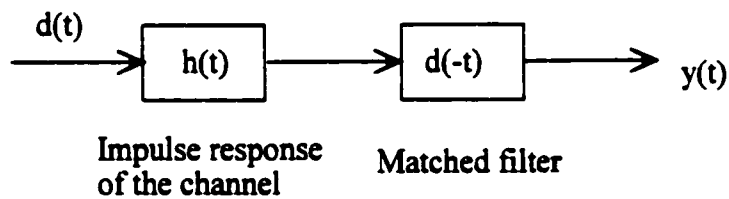
Multiplying both sides by $d*(\tau)$ gives

Figure 4.4 Channel Estimation By Correlation

$$d*(\tau)y(\tau+t) = d*(\tau)\int_{-\infty}^{+\infty} h(u)d((\tau+t)-u)du. \qquad (4.12)$$

Taking expectations over the ensembles gives

$$E[d^*(\tau)y(\tau+t)] = E[d^*(\tau)\int_{-\infty}^{+\infty} h(u)d((\tau+t)-u)]du . \qquad (4.13)$$

This can be rearranged to give

$$E[d^*(\tau)y(\tau+t)] = \int_{-\infty}^{+\infty} h(u)E[d^*(\tau)d(\tau+(t-u))]du . \qquad (4.14)$$

But those expectations can be replaced by the definitions of auto-correlation, $R_{dd}(t)$ and

cross-correlations $R_{dy}(t)$ to get

$$R_{dy}(t) = \int_{-\infty}^{+\infty} h(u)R_{dd}(t-u)du ,$$

or $\qquad\qquad R_{dy}(t) = h(t) * R_{dd}(t) . \qquad\qquad\qquad (4.15)$

Taking the Fourier transforms with respect to t gives

$$S_{dy}(f) = H(f)S_{dd}(f) . \qquad (4.16)$$

where $S_{dy}(f)$ is the cross-spectral density of $d(t)$ and $y(t)$, $S_{dd}(f)$ is the power spectral

density of $d(t)$, and $H(f)$ is the frequency response of $h(t)$. Rearranging gives

$$H(f) = \frac{S_{dy}(f)}{S_{dd}(f)} . \qquad (4.17)$$

If $d(t)$ is a white random noise process, then $S_{dd}(f)$ is a constant and it makes the

calculation of the frequency response come directly from Eq. 4.17.

Eq. 4.17 is true for continuous and discrete time signals. Considering discrete-time, we add a discrete matched filter d(-n) and the discrete output y(n) may be rewritten as

$$y(n) = d(n) * h(n) * d(-n),$$

$$= d(n) * d(-n) * h(n), \tag{4.18}$$

$$= \left[\sum_{k=1}^{N} d(n-k)d(k) \right] * h(n), \tag{4.19}$$

where N is the length of the training sequence and the first term in square brackets of Eq. 4.19 is actually the autocorrelation of the training sequence. d(n) will contain only {-1 1}. d(-n) means it is the time reversed form of d(n). d(-n) is also called a matched filter, which is matched to d(n). d(n) is designed to have the property

$$E[d(n-k)d(n)] = \begin{cases} 0 & k \neq 0, \\ 1 & k = 0. \end{cases} \tag{4.20}$$

Thus, if the length of sequence is infinite, the autocorrelation of the training sequence is just a scaled Kronecker delta function (see Fig. 4.5). We will obtain the important result

$$y(n) = Nh(n). \tag{4.21}$$

Because an optical communication system is a unipolar system, it means the transmitted signal bits are selected from the set of {0 1}. We still use reversed sequences in the form

{-1 1} for correlation which means that {-1 1} corresponds to {0 1} at the receiver. The difference with correlation using unipolar data is that we need twice the sequence length to get the same performance as the bipolar system. Eq. 4.21 will become

$$y(n) = \frac{N}{2} h(n).$$

(4.22)
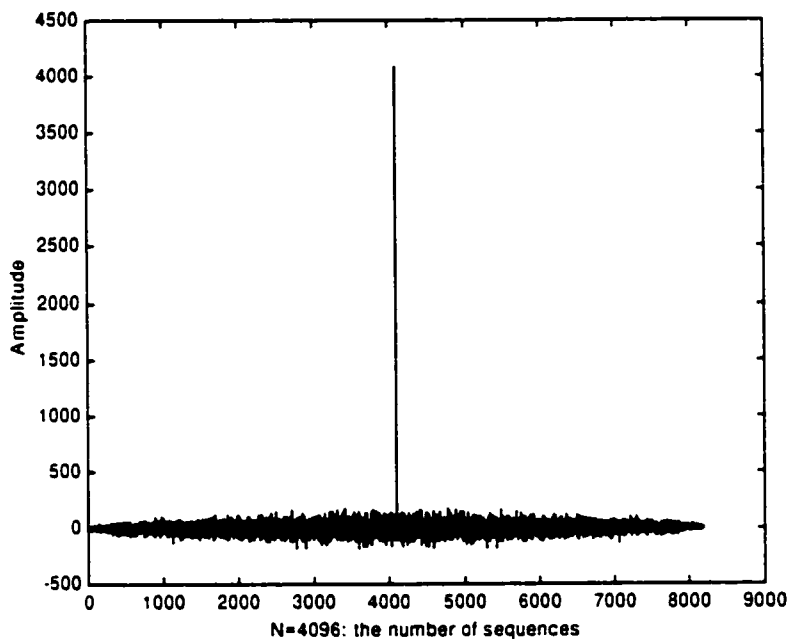
Figure 4.5 Convolution of the Training Sequences and Its Matched Filter

Fig. 4.6 demonstrates the channel identification by correlation. Comparing the original normalized impulse response of the channel with the estimated normalized impulse response of the channel by correlation, using 4096 training bits, they are similar. As N approaches infinity, they become identical. In real time, the number of training bits is limited, thus some error will result. This error will be discussed in section 4.6.

Original normalized impulse response of the channel

(a)

The impulse response of the channel after correlation

(b)

Time
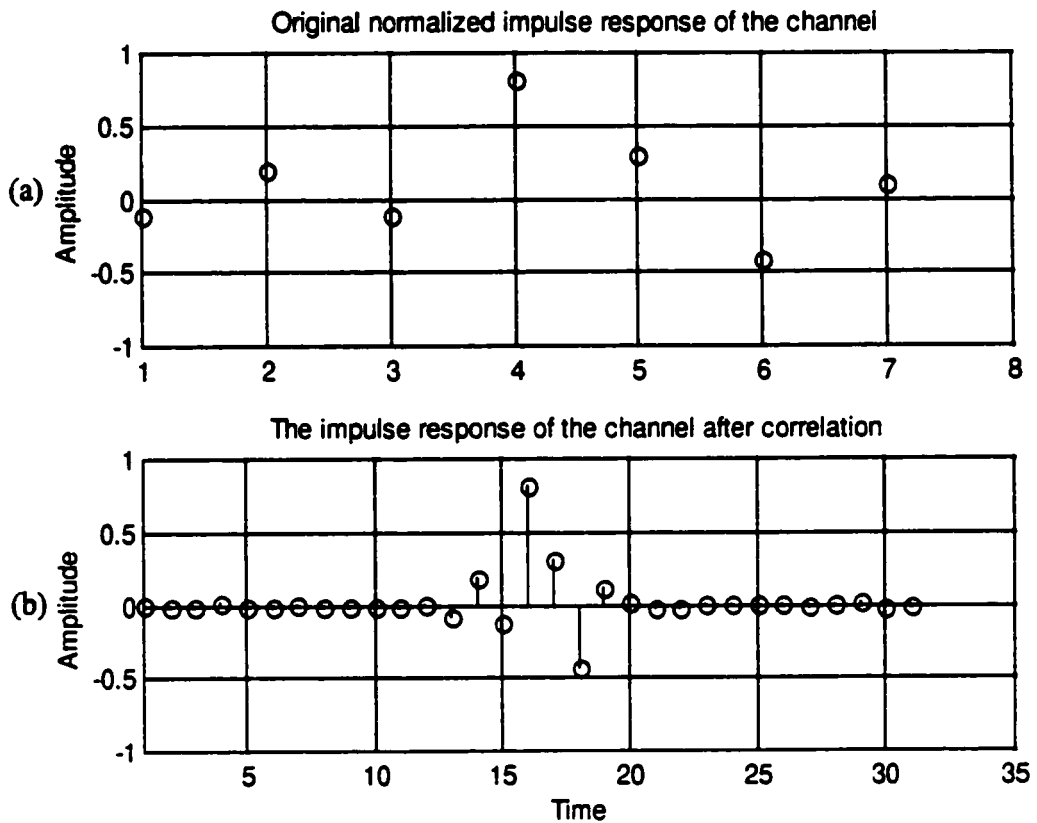
Figure 4.6 Demonstrate the Channel Identification by Correlation

4.5 Spread Spectrum

A major issue of concern in the study of digital communications is that of providing for the efficient utilization of bandwidth and power. The primary advantage of a spread-spectrum communication system is its ability to reject most interference whether it be unintentional interference or intentional interference.

The output signal-to-noise ratio, SNR_o, in terms of input signal-to-noise ratio, SNR_I, can be expressed as [31]

$$10\log_{10}(SNR)_o = 10\log_{10}(SNR)_I + 3 + 10\log_{10}(PG).$$ (4.23)

where $\quad$ PG = N . $\qquad\qquad\qquad\qquad\qquad\qquad\qquad$ (4.24)

The 3 dB term on the right-hand side of Eq. 4.23 accounts for the gain in SNR that is

obtained through the use of coherent detection (which presumes exact knowledge of the

signal phase by the receiver). This gain in SNR has nothing to do with the use of spread

spectrum. Rather, it is the last term, $10\log_{10}(PG)$, that is defined in Eq. 4.23, that is

referred to as the processing gain. Specifically, it represents the gain achieved by

processing a spread-spectrum signal over an unspread signal. Note that both the

processing gain PG and the spread factor N are equal to the PN sequence length. Thus,

the longer the PN sequence, the larger the processing gain. In the discrete case, N is just

the number of training bits.

We need to consider the processing gain because the power of the training signal is

much lower than the information-bearing signal (see section 4.3). For the purpose of

obtaining the impulse response of the channel, the information-bearing signal is noise

which needs to be suppressed. Fig. 4.7 demonstrates this idea. In this demonstration, the

power of the noise is 24 dB more than the power of the training sequences. In Fig. 4.7(b),

N equals 4096, corresponding to a processing gain of 36 dB. It is clear that the impulse

response is much different than the original impulse response of the channel. We owe

this error to the processing gain which is not big enough to suppress the noise; the error

comes from only 12dB gain above noise after correlation. This situation changes if the

training sequence length is increased to 65,536. Fig. 4.7(c) is much more similar to Fig.

4.7(a). The number 65,536 corresponds to a 48 dB gain. The signal is 24 dB above the

noise after correlation. That is the reason for the improvement. Ideally, if N is infinite,

there should be no error because we have infinite processing gain.
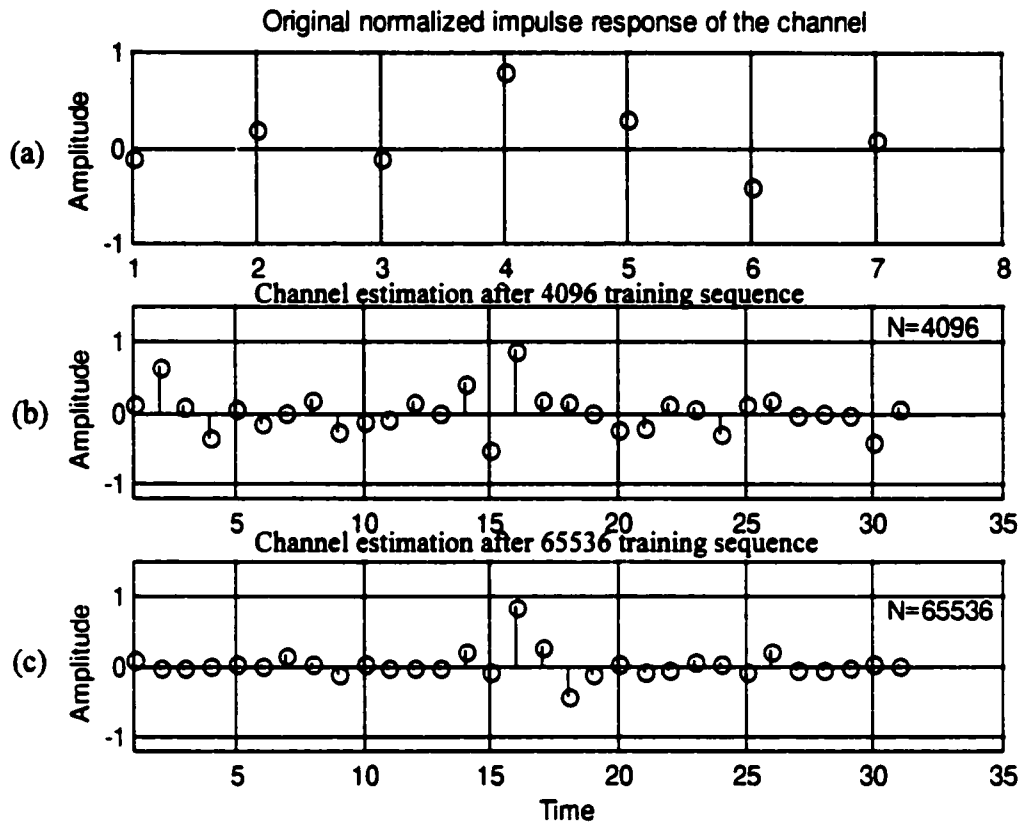
Figure 4.7 Effect of Processing Gain on System Identification

4.6 Quality Measure of Channel Estimate

There are some sources that cause the channel estimation error. One is the noise

from the photodetector and information-bearing signal. The second source comes from

the error between the autocorrelation of the PR training signal and a delta function. The

third is the time-varying characteristic of the channel. The fourth is the phase noise. We

will discuss them in detail.

Most of the problem lies in the fact that the PMD fluctuations relate to environmental changes, such as nonuniform stress and temperature variations, which occur on a time scale ranging from seconds to microseconds [17]; it is necessary to perform the channel identification within this time. In the simulation, the channel identification occurs in 0.2 microseconds, and the processing gain over 60 dB is also enough to suppress noise from the information-bearing signal and photodetector. In general, the longer the training sequence, the smaller the misadjustment. For a time-varying PMD channel, there is also a lag error, and the longer the training sequence, the worse the lag error becomes. It is a tradeoff.

Phase noise in the local oscillator is not a problem. From Eq. 4.9, we know

$$I_p(t) \propto \cos(\phi_s - \phi_{LO}) \ . \tag{4.25}$$

Because coherent detection is used to obtain the impulse response of the optical fiber channel with PMD, the phase difference between ϕ_s and ϕ_{LO} contributes to another form of time variation. The phase noise is not a problem because the local oscillator can be made sufficiently stable in order that the time variation caused by PMD is more significant.

To predict the performance of detectors that require an estimate of the channel response, an appropriate measure of the channel estimation error itself must be determined. The channel estimation error vector can be expressed as [7]

$$e_r(n) = h(n) - \bar{h}(n), \tag{4.26}$$

where $\bar{h}(n)$ is the estimated impulse response of the channel with PMD by correlation.

One measure of the quality of a channel estimate is the ratio of total energy in the channel

response to total mean squared estimation error. The signal-to-estimation error ratio

(SER) evaluates to

$$SER = \frac{\sum_{k=1}^{ml} |h(n)|^2}{\sum_{k=1}^{ml} |e_f(n)|^2} \quad , \tag{4.27}$$

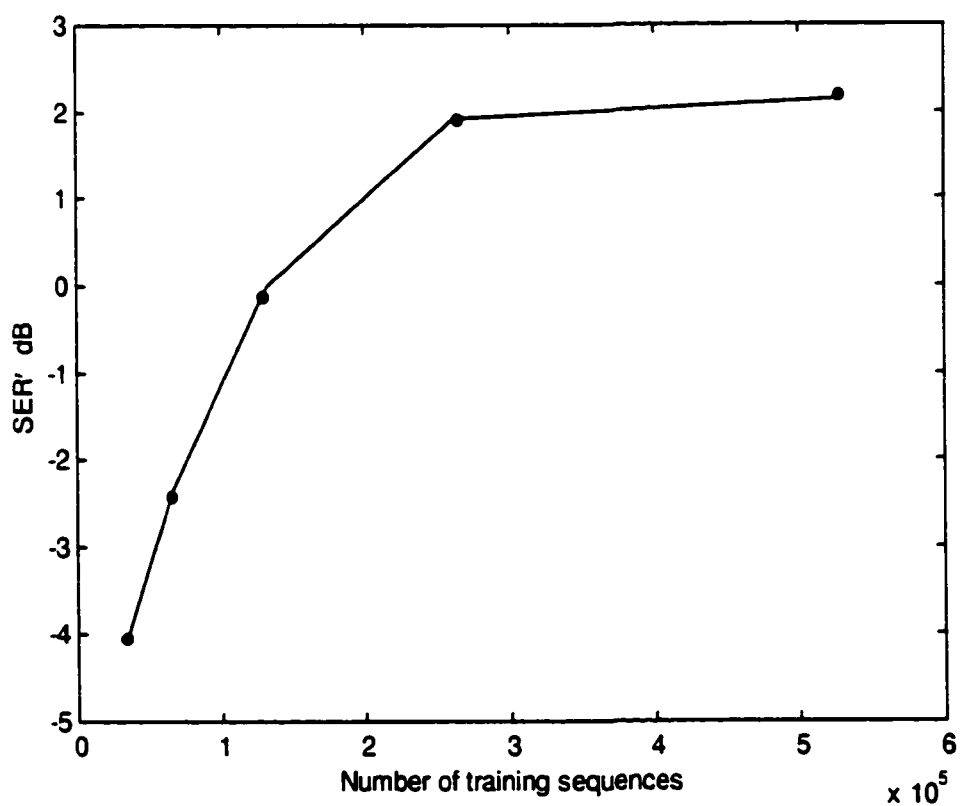
Figure 4.8 Normalized SER' Against the Length of Training Sequence

where m1 is the number of taps of the optical channel impulse response with PMD. Thus a normalized SER can be defined, and is given by

$$SER' = \frac{SER}{SNR},$$ (4.28)

where SNR is signal-to-noise ratio. This normalized SER is a convenient measure for comparing the quality of different training sequences. Generally, the higher the SER', the better the sequence for channel estimation purposes.

Fig. 4.8 shows the SER' against the length of training sequence. In this case, the SNR is 24 dB. The channel estimate's quality is considered to be good if SER' is greater than 1. In other words, SER > SNR.

4.7 Symbol Rate Tap Spacing and Fractional Rate Tap Spacing

An equalizer tap spacing equal to the symbol spacing has obvious advantages for the digital implementation of the equalizer, since it permits operation of the entire equalizer at the symbol clock rate, 1/T. However, unless there is no excess bandwidth, the synchronous structure does not, by itself, realize the optimum linear filter. The fact that the transfer function of the equalizer is periodic with period 1/T leads to two problems [12,28]:

1). the equalizer cannot suppress noise at frequencies outside the Nyquist band,

$$|f| \leq 1/(2T).$$

2). adequate equalization is not possible for all symbol clock phases, since the equalizer

cannot alter the relative magnitudes and phases of signal components which are more than $1/T$ apart in frequency and which in the course of sampling the equalizer output at clock rate $1/T$ become superimposed. A fractionally spaced equalizer (FSE) has the ability to compensate for an arbitrary receiver sampling phase.

The limitations of the symbol rate equalizer are most easily evident in the frequency domain. The signal spectrum of the equalizer is

$$H_T(f) = \sum_{k=1}^{m} w_k e^{-j2\pi fkT} .$$

(4.29)

It is clear from the above relationship that the symbol rate equalizer can only compensate for the frequency characteristics of the aliased received signal.

Since the frequency response of the FSE ($T' < T$) is

$$H_{T'}(f) = \sum_{k=1}^{m} w_k e^{-j2\pi fkT'} ,$$

(4.30)

we observe that the FSE compensates for the channel distortion in the received signal before the aliasing effects due to symbol rate sampling. In other words, $H_{T'}(f)$ can compensate for any arbitrary timing phase. $T/2$-spaced equalizer is used in many applications and we choose $T'=T/2$ in this thesis. It must be noted that although a FSE is a T'-spaced equalizer, the output is still sampled at the symbol rate $1/T$.

Chapter 5

Equalization Analyses

This chapter will present the technique to calculate the coefficients of the equalizer after the channel identification is obtained. Simulation results of equalization will be given in terms of eye pattern and bit error rate. Quasi-analytical calculations are used to estimate the bit error rate because they have an enormous saving in calculation compared to exhaustive bit error rate simulations. A discussion will follow.

5.1 Equalization Coefficients

There are two methods to calculate the coefficients of the optical transversal filter based on a known impulse response of the channel, the Wiener-Hopf equation and the LMS algorithm. This inverse filtering problem may be stated as follows. Given the input $u(n)$ and the output of a filter $h(n)$, which has a z transform of $H(z)$, determine the inverse filter $h_r(n)$, such that

$$H_r(z)H(z) = 1. \tag{5.1}$$

where $H_r(z)$ is the z transform of $h_r(n)$. The solution is to transmit a known sequence $d(n)$ into a channel $h(n)$ followed by a filter $h_r(n)$, to get the estimate of the signal $\hat{d}(n)$. The performance criterion is the mean squared error (MSE)

$$J = E[(d(n) - \bar{d}(n))^2].$$ (5.2)

Minimizing the MSE allows an efficient method to determine the optimum coefficients of the equalizer [46]. Fig. 5.1 shows this problem, where D is the time delay.
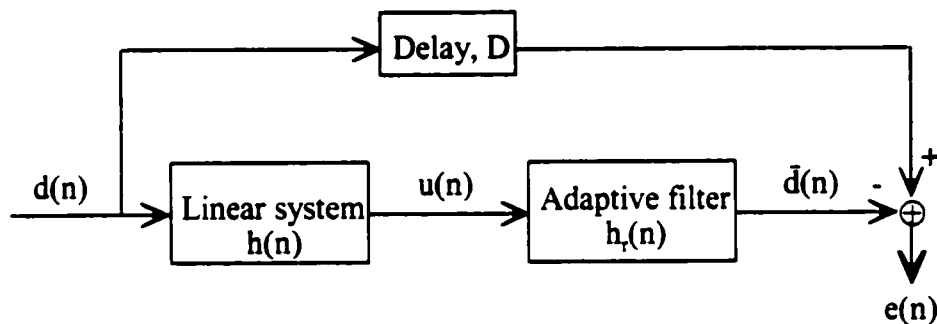
Figure 5.1 Calculating Equalization Coefficients

5.2 LMS Algorithm

The other method used to obtain coefficients of the adaptive filter is the least mean square (LMS) algorithm [31]. As in Fig. 5.1, the known input sequence u(n) applied to this equalizer is produced by the transmission of a random binary sequence d(n) through a known channel whose impulse response is h(n). From channel identification, the question is how to get the coefficients of the equalizer filter $h_r(n)$. To simplify notational matters, we let

$$d_n = d(n),$$

$$\overline{d}_n = \overline{d}(n), \text{ and} \tag{5.3}$$

$$u_{n-k} = u(n-k). \tag{5,4}$$

Then, the output $\overline{d}(n)$ of the equalizer in response to the input sequence $d(n)$ is defined by the discrete convolution sum (see Fig. 5.1),

$$\overline{d}_n = \sum_{k=1}^{m} w_k u_{n-k}, \tag{5.5}$$

where w_k is the weight of the k-th tap. The input sequence u_n is assumed to have finite energy.

Let e_n denote the error signal defined as the difference between the desired response $d(n)$ and the actual response $\overline{d}(n)$ of the equalizer, as shown by

$$e_n = d_n - \overline{d}_n. \tag{5.6}$$

Then, a criterion commonly used in practice is the mean-square error, defined by the cost function

$$\varepsilon = E[e_n^2]. \tag{5.7}$$

The optimality condition for minimum mean square error may now be expressed simply as

$$\frac{\partial \varepsilon}{\partial w_k} = 0. \tag{5.8}$$

In a corresponding fashion, we use the estimate $\hat{w}_k(n)$ in place of the tap weight w_k. A

recursive formula for updating the weights $\hat{w}_k(n)$ of the equalizer is expressed as follows

$$\hat{w}_k(n+1) = \hat{w}_k(n) + \mu e_n u_{n-k} .$$ (5.9)

This algorithm is known as the least mean square (LMS) algorithm. Viewing n as the

index for the previous iteration, $\mu e_n u_{n-k}$ is the correction applied to it to compute the

updated value, and μ is a small positive constant called the step-size parameter.

The LMS algorithm is summarized as follows.

1. Initialize the algorithm by setting $\hat{w}_1 = 0$, which means setting all the tap-weights of

   the equalizer to zero at n=1.

2. For n=1,2,3, ... , compute

$$\bar{d}_n = u_n^T \hat{w}_n ,$$

$$e_n = d_n - \bar{d}_n ,$$

$$\hat{w}_{n+1} = \hat{w}_n + \mu e_n u_n .$$ (5.10)

3. Continue the computation until steady-state conditions are reached.

The LMS algorithm is often used first in a training mode followed by a decision-

directed mode. However, here the decision-directed mode is not needed. We are

interested in finding the optimal coefficients, w_k. One complex method is to solve the

Wiener-Hopf equation. Alternatively, we are using the LMS algorithm to calculate w_k

iteratively by feeding PR data into a filter whose impulse response is the known channel

estimate.
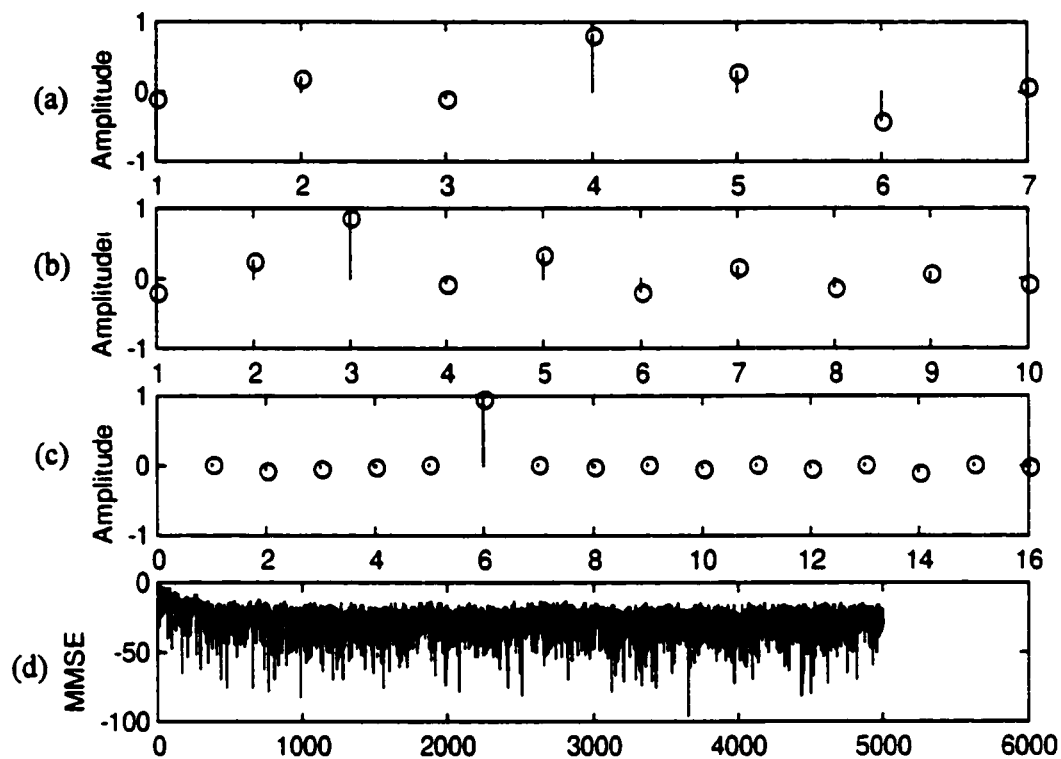
Figure 5.2 Demonstrating Inverse Filtering or Deconvolution

Fig. 5.2 shows the deconvolution or the coefficient calculation of the inverse filter

using the LMS algorithm. Fig. 5.2(a) shows the original impulse response of the channel

normalized to have unit energy. Fig 5.2(b) shows the calculated inverse filter coefficients

from the LMS algorithm, and the convolution of the channel and inverse filter is shown in

Fig 5.2(c). The learning curve is shown in Fig. 5.2(d), $\mu=0.025$.

5.3 Bit Error Rate Estimator

Over the past two decades, it has become increasingly common to resort to computer aided techniques to estimate the performance of digital communication systems. This trend has been particularly apparent in optical fiber communication. The definition of performance almost universally used is the bit error rate (BER) or the bit error probability. There are a number of ways such as Monte Carlo simulation and quasi-analytical calculations to arrive at an estimate of BER, each with its own advantages and disadvantages [20]. The Monte Carlo method is the least restrictive but the costliest in terms of computer time. Because optical fiber communication is a very low bit error rate system, which can be smaller than 10^{-10}, the Monte Carlo method is not practical in simulation. The quasi-analytical method combines a noiseless simulation with an analytical representation of noise. Also, it is by far the most rapid and in a linear channel is exact, insofar as the effects of Gaussian noise are concerned. Because of its speed, this method is also suitable for sensitivity studies. The PDF statistics of the noise are not sufficient in themselves to compute the BER because the system distortion from PMD must be considered. In this approach, the simulation itself computes the effect of PMD distortion in the absence of noise, and then superimposes the noise on the noiseless waveform. To clarify the method, refer to Fig. 5.3. Fig. 5.3(a) shows a hypothetical transmitted bit stream, while Fig. 5.3(b) shows the corresponding noiseless received waveform at the input to the decision device. The value of this waveform at the k-th sampling instant is denoted v_k. When the noise is superimposed, the probability that the resulting sum will produce an error is, P_k, well approximated by:

$$P_k = \text{Prob}[\text{noise} > v_k] = \int\limits_{v_k}^{\infty} f_n dn \qquad v_k \leq 0,$$

$$= \text{Prob}[\text{noise} < v_k] = \int\limits_{-\infty}^{v_k} f_n dn \qquad v_k > 0,$$

(5.11)

where f_n is the probability density function of the noise. For the Gaussian distributed

noise in this thesis, P_k can be written as

$$P_k = \frac{1}{2} \text{erfc}(\frac{Q}{\sqrt{2}}),$$

(5.12)

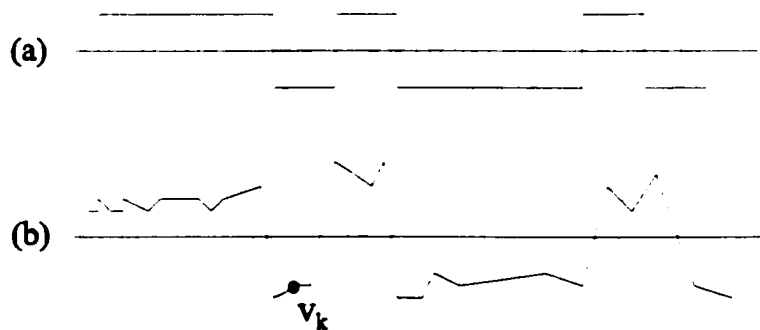where erfc stands for the complimentary error function, defined as

(a)

(b)

v_k

Figure 5.3 Illustration of Quasi-analytical Method

$$erfc(x) = \frac{2}{\sqrt{\pi}} \int_{x}^{\infty} exp(-y^2)dy , \qquad (5.13)$$

and $\qquad Q = \frac{v_k}{\sigma},$ \qquad (5.14)

where σ is the variance of the noise at the receiver. The total (average) probability of

error is just

$$P_e = (\frac{1}{N1})\sum_{k=1}^{N1} P_k , \qquad (5.15)$$

where N1 is the length of the sequences observed. Also implied in this procedure is the

independence of successive noise samples.

In this approach, as implied above, the simulation itself computes the noiseless

waveform, i.e. the sequence v_k. Thus, the quasi-analytical description arises from the fact

that the individual computations (Eq. 5.11) can be expressed in a definite mathematical

form. If there are no fluctuations in the sampled signal amplitude, it would take exactly

one computation of the type (Eq. 5.11) to obtain the BER. If there is no knowledge of the

noise statistics, one would be obliged to use a Monte Carlo approach, and even with the

distortionless assumption on the signal we would still need to run a relatively lengthy

simulation to obtain the BER estimate. We can see, therefore, that assumption of the

noise statistics leads to a great reduction in computing efforts. Realistically, of course,

there will be fluctuations in signal amplitude, and these fluctuations will generally be a

function of the particular sequence transmitted, as in the case of PMD. Thus, if the noise

introduced by the receiver is simulated as Gaussian noise with mean zero and variance σ^2,

performance estimates can be handled by a closed-form analysis. Short PR codes (on the

order of 1024 or 4096 bits) can be used to evaluate the combined effects of ISI from PMD

and Gaussian noise, thus minimizing the required computer time.

5.4 Simulation Results

The first set of simulations was performed for a moderate distortion, DGD equals

72 ps, less than the bit spacing 100 ps. For these simulations, the number of taps were

chosen large enough to reach the desired level of convergence. The number of training

bits is 2×10^6. The number of samples per symbol is 10. The input signal is formed from

raised cosine pulses. The power of the training signal is chosen to be 30 dB lower than

the power of information-bearing signal. For the bandwidth considered, a T/2- tap spaced

FSE is used to compensate for PMD. The advantage of the T/2 spacing is that the

receiver performance is almost independent of the receiver sampling phase.

The steps to obtain the simulation results are as follows.

1. Simulate the channel using PMD model detailed in chapter 3. In our simulation, we
   use 500 segments to generate dispersion.

2. Obtain the impulse response of the channel using the correlation method described in
   chapter 4.

3. Calculate the inverse coefficients of the optical filter using the LMS algorithm.

4. Use the optical equalizer to compensate for the distortion. Results are displayed in

terms of eye patterns, pulse shapes and BER.

Fig. 5.4 shows the pulse before and after compensation. In this case, DGD=72 ps

and γ=0.5 which is the worst power ratio between the fastest and the slowest PSPs. Fig.

5.4(a) is the input raised cosine, shown for 2^6 pulses at the transmitter. In Fig. 5.4(b), we

show the output pulses after the PMD distorted channel at the receiver. One can see the

PMD distortion by comparing Fig. 5.4(a) with Fig. 5.4(b). After a 10-tap optical inverse

filter, we obtained the equalized pulses, shown in Fig. 5.4(c). Note that the process of
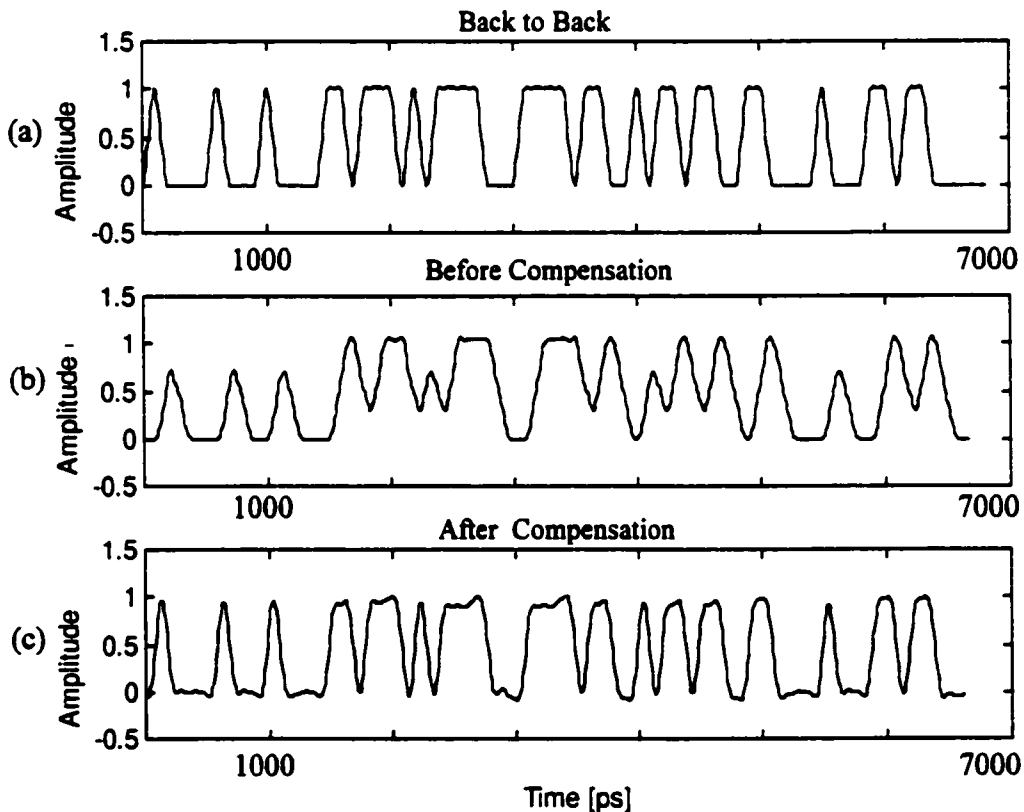
Figure 5.4 Simulation of First-Order PMD Compensation in a
10 Gb/s Optical NRZ Signal (DGD=72 ps γ=0.5)

equalizing is completed in 0.2 ms, which is required in order to compensate for the effect of time varying PMD.

The eye pattern technique is a simple but powerful measurement method for assessing the data-handing ability of a digital transmission system. By superimposing the pulses of Fig. 5.4, we calculate the eye diagram and the results are shown in Fig. 5.5 which shows the changes in diagrams. Fig. 5.5(a) is the eye diagram before the channel, Fig. 5.5(b) is the eye diagram of the output pulse after PMD distortion, while Fig. 5.5(c)
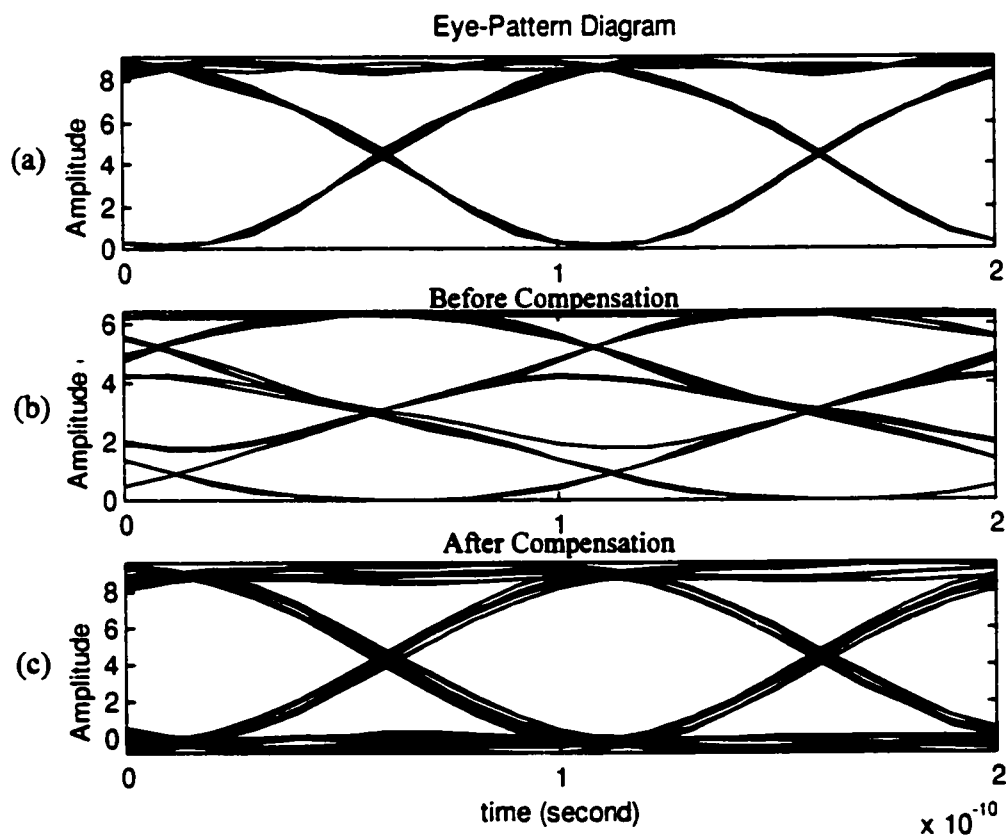
Figure 5.5 Eye Pattern Before and after Compensation
(DGD=72 ps γ=0.5)

shows the improvement after compensation. After compensation the eye is much more

open than before equalization. To compute the bit error rate at the receiver, a QA

approach, described in section 5.4, is used so that the amount of simulation time required

to obtain an accurate estimate for the probability of error can be reduced. The receiver

noise is modeled as Gaussian distributed. Short PR codes, 2048 bits are used to evaluate

the performance.

Fig. 5.6 shows the effects of compensation in the frequency domain. It consists of

the spectra of the launched signal, the received signal before compensation and the
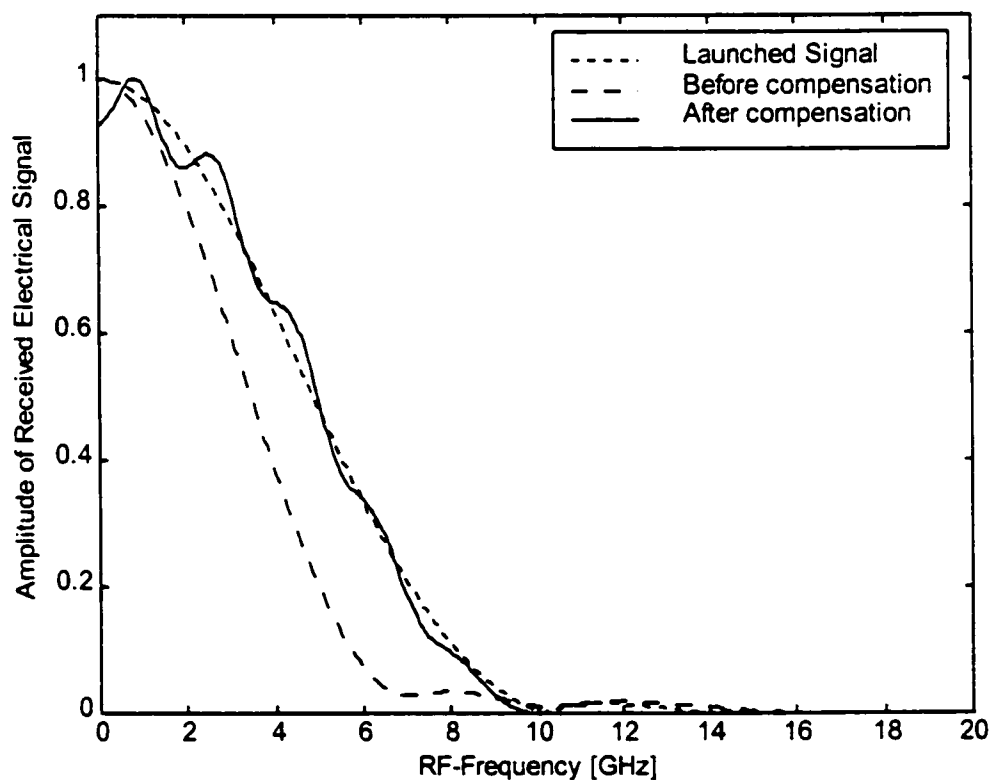
Figure 5.6 Simulation of RF Spectra of Received Signals Before and After
Compensation (DGD=72 ps γ=0.5)

received signal after compensation.

Fig. 5.7 shows the bit error rate before and after compensation. These are the bit error rates for the cases of before compensation, after compensation and back to back, meaning no optical channel present. From the diagram we can see the improvement. It can be seen at a BER=10^{-9}, the power penalty is about 8 dB before compensation; the power penalty is reduced to 0.2 dB after compensation. Thus a penalty reduction of 7.8 dB is demonstrated. In this case the delay between the slow and fast PSPs is 72 ps and the power splitting ratio is $\gamma=0.5$.
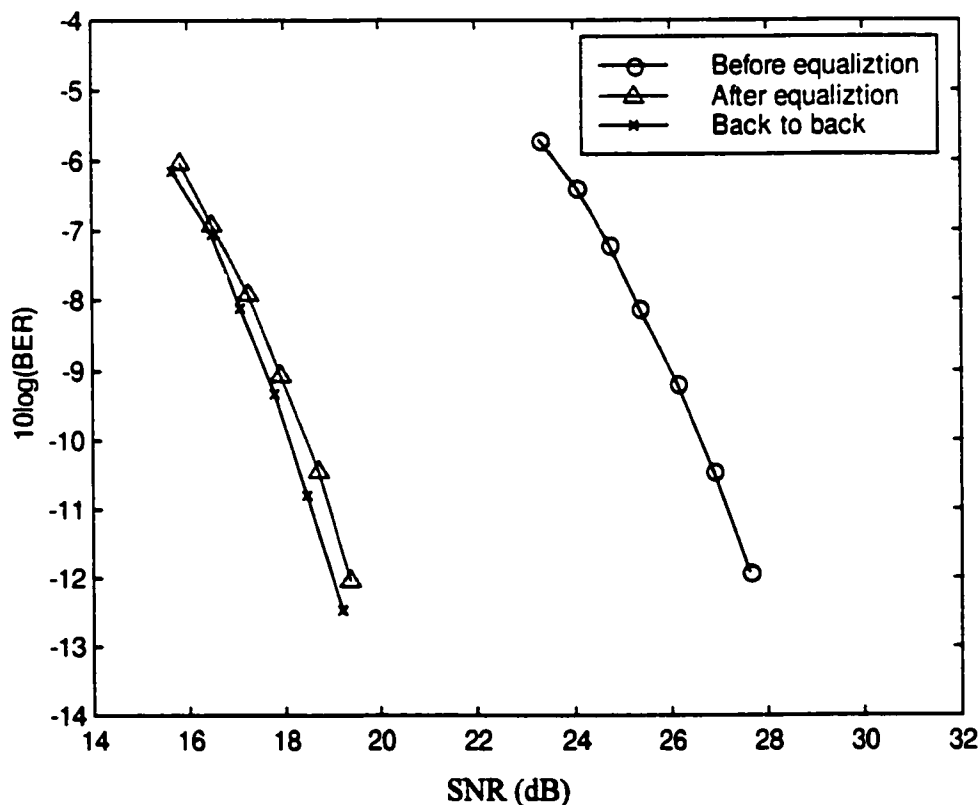
Figure 5.7 Simulation of Bit Error Rate Before and After Compensation (DGD=72 ps $\gamma=0.5$)

To demonstrate the ability of this technique to compensate large DGD, more than

100 ps, we simulated the severe distortion. In this case, the DGD is 114 ps and γ=0.5.

Fig. 5.8(a) is similar to Fig 5.5(b) and Fig. 5.8(b) is similar to Fig 5.5(c) except for

the difference in DGD. We can see this technique also works when the eye is closed.

Before compensation the eye was closed; see Fig. 5.8(a). After a 15-tap optical filter, the

eye is open; see Fig. 5.8(b). Other parameters are same as the case when DGD=72 ps.

Fig. 5.9 is similar to Fig. 5.4 except that PMD distortion is much more severe.

Fig. 5.9(a) shows the input pulses at the transmitter. The distorted output pulses are

shown in Fig. 5.9(b) whose eye pattern is Fig. 5.8(a); the compensated output pulses are
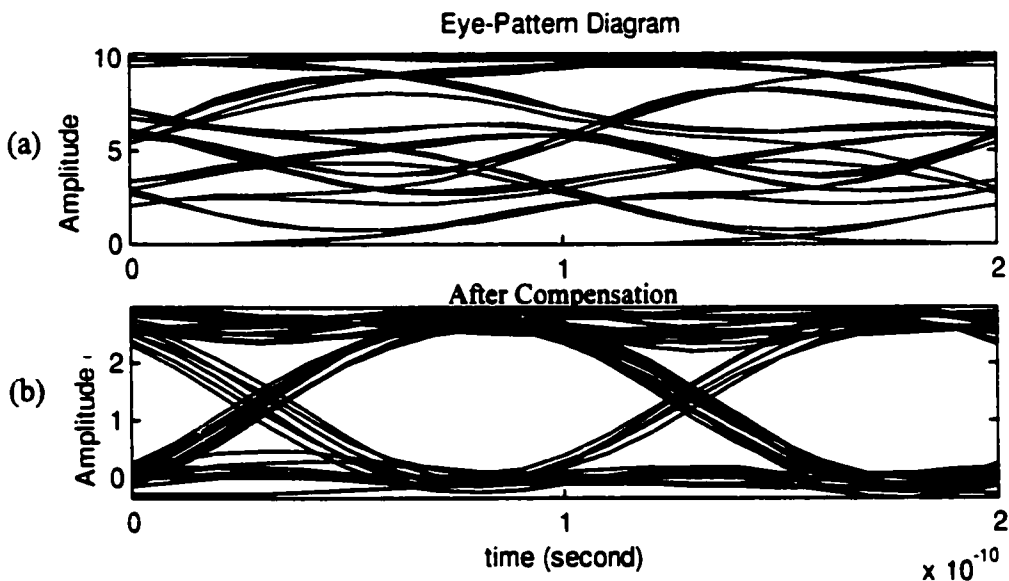
Figure 5.8 Eye Pattern Before and After Compensation
(DGD=114 ps γ=0.5)

shown in Fig. 5.9(c) whose eye pattern is Fig. 5.8(b).

We need more equalizer taps when the distortion is worse, 15 taps are used in the case of DGD=114 ps compared to 10 taps in the case of DGD=72 ps. It can be concluded from the above simulations that this technique works well no matter how much distortion is present, provided we have enough taps.
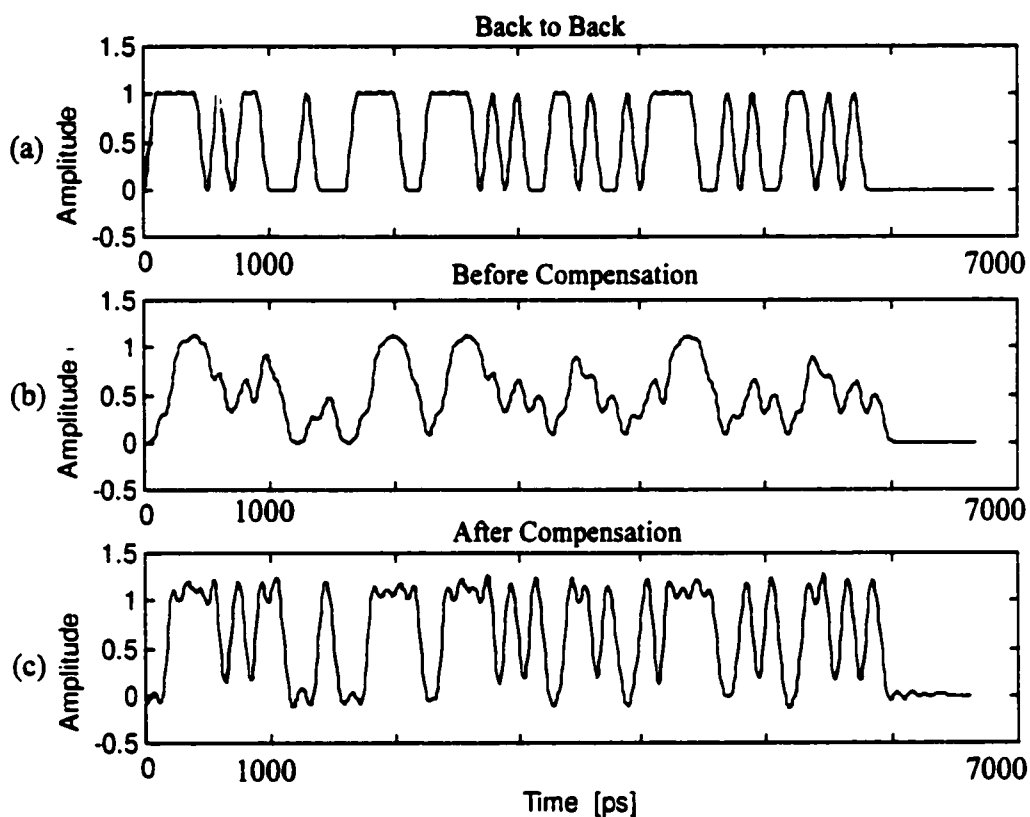
Figure 5.9 Simulation of First-Order PMD Compensation in a 10 Gb/s Optical NRZ Signal (DGD=114 ps γ=0.5)

5.5 Discussion

From the previously described two cases of distortion, we demonstrated the

success of compensation based on channel identification to compensate for the typical

PMD distortion. The results are general even though this thesis is confined to specific

values of DGD in the fiber simulation and a particular raised cosine shaped input signal.

To keep the phase information, coherent detection is used in channel identification. A

T/2 spaced equalizer sampling rate is needed, while the output sampling rate is still 100

ps. The drawback of an FSE is that more taps are needed compared with a symbol spaced

equalizer. The impulse response of the optical channel with PMD can change slowly due

to temperature variations on the order of a few seconds. In this case tracking of the

changes by the equalizer is not difficult.

Chapter 6

Conclusions

6.1 Summary

This thesis has presented the ability of equalizers to compensate first-order PMD. This technique can be easily extended to second-order or higher-order PMD, if the optical fiber is assumed to be a linear system. In other words, this thesis proposed a method to reduce ISI from first-order, second-order, or higher-order PMD simultaneously.

Through numerical simulation, the model of an optical fiber with first-order PMD was studied. The eye patterns were analysed with various levels of PMD distortion which showed clearly that this distortion heavily depends on PSPs and the power ratio between the two PSPs. The statistics of DGD are also given. The difficulty of PMD compensation arises from its time varying characteristics.

The details of how to obtain the impulse response of the optical channel with PMD were discussed. This channel identification is based on correlation with the training sequences. The requirement of the training with sequences in a limited time was also considered. Successful compensation of PMD in terms of eye pattern and bit error rate was proved. The price to be paid for the compensation is that coherent detection is needed in the compensator to keep the phase information.

Deconvolution is needed to obtain the coefficients of the optical equalizer filter after obtaining the impulse response of the channel. An LMS algorithm is used in

implementing the deconvolution.

A fractional rate tap spacing rather than a symbol rate tap spacing equalizer was used due to bandwidth considerations. The advantage of a fractional rate tap spacing comes from its ability to compensate for an arbitrary receiver sampling phase. However, it needs more taps than the symbol rate tap spacing filter.

Moreover, the benefit of using an optical transversal filter was studied because of the large available bandwidth of optical waveguides. This filter was developed for ultrahigh-speed real time optical signal processing.

6.2 Future Research

Throughout this thesis the influence of the chromatic dispersion introduced by the fiber and polarization dependent losses were neglected. The influence of these factors should be considered in a more thorough analysis.

The PMD model is restricted to first order. A second order PMD model is not presented in this thesis.

This thesis is confined to specific values of DGD of the fiber simulation and to a particular raised cosine shaped input signal. The impact of a change in these factors has yet to be fully assessed. A time varying PMD model is too complicated to be investigated in this thesis.

Although we showed successful compensation through simulation, the simulation results need to be verified by future experiments.

REFERENCES

[1] Ivan P.Kaminow, Thomas L.Koch, *Optical Fiber Telecommunications*, Chapter 6, Academic Press, 1997.

[2] Frank Bruyere, "Impact of first- and second-order PMD in optical digital transmission systems", *Optical Fiber Technology*, pp. 269-280, 1996.

[3] C.D.Poole and R.E.Wagner, "Phenomenological approach to polarization dispersion in long single-mode fibers", *Electron. Lett.*, vol. 22, pp. 1029-1030, 1986.

[4] C.D.Poole, R.W.Tkach, A.R.Chraplyvy, D.A.Fishman, "Fading in lightwave systems due to polarization-mode dispersion", *IEEE Photonics Technology*, vol. 3, January, 1991.

[5] Agrawal P.Agrawal, *Fiber-optic communication systems*, John Wiley & Sons, Inc., 2nd edition, 1997.

[6] Koji Sasayama, Masayuki Okuno, Keishi Habara, "Coherent optical transversal filter using silica-based waveguides for high-speed signal processing", *Journal of Lightwave Technology*, vol. 9, pp. 1225-1230, October, 1991.

[7] S.N.Crozier, D.D.Falconer, S.A.Mahmoud, "Least sum of squared errors(LSSE) channel estimation", *IEE Proceedings-f*, vol. 138, pp. 371-378, August, 1991.

[8] H.Bulow, R.Ballentin, W.Baumert, G.Maisonneuve, G.Thielecke, T.Wehren, "Adaptive PMD mitigation at 10Gbit/s using an electronic SiGe equalizer IC", *Proc. ECOC 99*, France, Sep. 1999.

[9] Fred Heismann, "Tutorial: polarization mode dispersion: fundamentals and impact

on optical communication systems", *ECOC 98*, Madrid, Spain, 1998.

[10] Henning Bulow and Gustav Ceith, "Temporal dynamics of error-rate degradation indued by polarization mode dispersion fluctuation of a field fiber link", *ECOC 97*, 1997.

[11] M.Kavehard and J.Salz, "Cross-polarization cancellation and equalization in digital transmission over dually polarized multipath fading channels", *AT&T Technical Journal*, pp. 2211-2244, December, 1985.

[12] R.D.Gitlin and S.B.Weinstein, "Fractionally-spaced equalization: an improved digital transversal equalizer", *The Bell System Technical Journal*, pp. 275-296, February, 1981.

[13] Fred Heismann, Daniel A.Fishman, David L.Wilson, "Automatic compensation of first-order polarization mode dispersion in a 10Gb/s transmission system", *Proc. ECOC 98*, Madrid, Spain, Sep. 1998.

[14] R.E.Wagner, A.F.Elrefaie, "Polarization-dispersion limitations in lightwave systems", *OFC 88*, 1998.

[15] Cristian Francia, Denis Penickx et. al., "Time impulse response of second order PMD in single-mode fibers", *ECOC 98*, Madrid, Spain, 1998

[16] Aly F.Elrefaie, J.Keith Townsend, et. al., "Computer simulation of digital lightwave links", *IEEE J. Select. Areas in Commun.*, vol. 6, No.1, pp. 94-105, January 1988.

[17] Agrawal P.Agrawal, *Fiber-optic communication systems*, John Wiley & Sons, Inc., 1992.

[18] Jack H.Winters, Mario A.Santoro, "Experimental equalization of polarization dispersion", *IEEE Photonics Technology*, vol. 2, pp. 591-593, August 1990.

[19] Jack H.Winters, "Equalization in coherent lightwave systems using a fractionally

spaced equalizer", *Journal of Lightwave Technology*, vol. 8, pp. 1487-1491,

October, 1990.

[20] Michel C.Jeruchim, "Techniques for estimating the bit error rate in the simulation

of digital communication systems", *IEEE J. Select. Areas in Commun.*, vol. sac-2,

pp. 153-170, January, 1984.

[21] Dieter Schlump, Berthold Wedding, et. al., "Electrical equalization of PMD and

chromatic dispersion induced distortion after 100km standard fiber at 10Gbit/s",

ECOC 98, Madrid, Spain.

[22] Reinhold Noe, David Sandel, et. al., "Polarization mode dispersion compensation

at 10, 20, and 40 Gb/s with various optical equalizers", *Journal of Lightwave

Technology*, vol. 17, pp. 1602-1616, Sep. 1999.

[23] J.P.Elbers, C.Glingener, et. al., "Modelling of polarization mode dispersion in

single mode fibers", *Electron. Lett.*, vol.33, pp. 1894-1895, Oct. 1997.

[24] Hideyuki Sotobayashi, Ken-ichi Kitayama, "Transfer response measurements of a

programmable bipolar optical transversal filter by using the ASE noise of an

EDFA", *IEEE Photonics Technology*, vol.11, pp. 871-873, July, 1999.

[25] John Cameron, Liang Chen, et. al., "Time evolution of polarization mode

dispersion in optical fibers", *IEEE Photonics Technology*, vol. 10, pp. 1265-1267,

Sep. 1998.

[26] Jack H.Winters, Richard D.Gitlin, "Electrical signal processing techniques in long-

haul fiber-optic systems", *IEEE Trans. on Commun.*, vol. 38, pp. 1439-1453,

Sep. 1998.

[27] Jack H.Winters, Richard D.Gitlin and Sanjay Kasturia, "Reducing the effects of

transmission impairments in digital fiber optic systems", *IEEE Commun. Magaz.*, June, 1993.

[28] Gottfried Ungerboeck, "Fractional tap-spacing equalizer and consequences for clock recovery in data modems", *IEEE Trans. on Commun.*, vol. Com-24, pp. 856-864, August, 1976.

[29] C.D.Poole and C.R.Giles, "Polarization-dependent pulse compression and broadening due to polarization dispersion in dispersion-shifted fiber", *Optic Letters*, vol. 13, pp. 155-157, Feb. 1988.

[30] Anjan Ghosh, Jim Barner and Palacharla Paparao, "Design of least-mean-square based adaptive optical equalizers", *Optics Communication*, vol. 91, pp. 280-292, 1992.

[31] Simon Haykin, *Communication Systems*, John Wiley & Sons, Inc., third edition, 1994.

[32] M.W.Chbat, J-P. Soigne, et. al., "Long term field demonstration of optical PMD compensation on an installed OC-192 link", *OFC 99*.

[33] F.Curti, B.Daino, et. al., "Concatenation of polarization dispersion in single-mode fibers", *Electron. Lett.*, vol. 25, pp. 290-292, Feb. 1989.

[34] C.D.Poole, Neal S.Bergano, et. al., "Polarization dispersion and principle states in a 147-km undersea lightwave cable", *Journal of Lightwave Technology*, vol. 6, pp. 1185-1190, July, 1988.

[35] Jack H.Winters, Sanjay Kasturia, "Adaptive nonlinear cancellation for high-speed fiber-optic systems", *Journal of Lightwave Technology*, vol. 10, pp. 971-977, July, 1992.

[36] C.D.Poole, J.H.Winters and J.A.Nagel, "Dynamical equation for polarization

dispersion", *Optics Letters*, vol. 16, pp. 372-374, March, 1991.

[37]   Brent R.Petersen, *Communication Notes*, University of New Brunswick, May,
        2000.

[38]   B.L.Kasper, "Equalization of multimode optical fiber systems", *The Bell System
        Technical Journal*, vol. 61, pp. 1367-1387, Sep. 1982.

[39]   J.Zhou and M.J.O'Mahony, "Optical transmission system penalties due to fiber
        polarization mode dispersion", *IEEE Photonics Technology*, vol. 6, pp. 1265-1267,
        October, 1994.

[40]   Eric UDD., *Fiber Optic Sensor: An introduction for Engineering and Scientists*,
        John Wiley & Sons, Inc., Chapter 8, 1991.

[41]   *Communications Toolbox for Use with Matlab*, The MathWorks, Inc., 1996.

[42]   Franco Curti, Benedetto Daino, et. al., "Statistical treatment of the evolution of the
        principal states of polarization in single-mode fibers", *Journal of Lightwave
        Technology*, vol. 8, pp. 1162-1165, August, 1990.

[43]   B.W.Hakki, "Polarization mode dispersion compensation by phase diversity
        detection", *IEEE Photonics Technology*, vol. 9, pp. 121-123, January, 1997.

[44]   Brent R. Petersen, "Equalization in cyclostationary interference", *Ph.D thesis*,
        Carleton University, October, 1991.

[45]   J.Capmany and J.Cascon, "Optical programmable transversal filters using fiber
        amplifiers", *Electron. Lett.*, 1992.

[46]   Simon Haykin, *Adaptive Filter Theory*, Prentice-Hall, Inc., third edition, 1996.

[47]   J.G.Proakis, *Digital Communication*, New York, McGraw-Hill, second edition,
        1983.

[48]   Brent R.Petersen, *EE 6533 Topics in Communication Notes*, University of New

Brunswick, 2000.

[49]   Theodore S.Rappaport, *Wireless Communication Principles and Practice*, New

Jersey, USA, Prentice-Hall, 1996.

[50]   Gred Keier, *Optical Fiber Communications*, McGraw-Hill, Inc., second edition,

1991.

[51]   Jack H.Winters, Zygmunt Haas, Mario A.Santoro, Alan, H.Gnauck, "Optical

equalization of polarization dispersion", *Multigigabit Fiber Communication*,

pp. 346-356, 1992.

[52]   M.W.Chbat, J-P.Soigne, et. al., "Long term field demonstration of optical PMD

compensation on installed OC-192 link", *OFC 99*.

Appendix A

Appendix A presents the Matlab source code used for the simulation of PMD and compensation. The entire system named "Sys.m" is used to simulate the distortion with PMD and the effect of the equalization. The purpose of these two subroutines called "Iden.m" and "Equali.m" is channel estimation by correlation and calculation of the optical filter coefficients, respectively. An additional function "Pmd.m" is included to model the impulse response of the optical channel with PMD. Finally the "DGD.m" program permits the search for the PSPs and DGD calculation.

```
% ---------------- System.m (DGD=72 ps) ----------------
% Simulation of PMD, and its compensation based on channel estimation.

clear all;
global deltat;
deltat=72*1e-12;          % 75ps
fsample=10*10e9;
t0=clock;
N=2^10;
Nin=2^20;                 % number of training sequence
fcutoff=2.*5e9;
beta=(15+45)*pi/180;


% ----------Model of PMD------------
[t,hr,hi]=pmd(fsample,N,deltat,fcutoff);
hr11=hr(1,:);
hr21=hr(2,:);
hr12=hr(3,:);
hr22=hr(4,:);


% -------Normalized----------
inputh=((1))*cos(beta);
inputv=((1))*sin(beta);
outputho=conv(inputh,hr11)+conv(inputv,hr21);
outputvo=conv(inputh,hr12)+conv(inputv,hr22);
normal=sqrt(sum(outputho.^2)+sum(outputvo.^2));
hr11=hr11/normal;
hr21=hr21/normal;
hr12=hr12/normal;
hr22=hr22/normal;


% ----------Sample ----------
a=randint(2^6-1,1,2);
a=[a'zeros(1,5)];
input=(rcosflt(a,10e9,10*10e9,'normal',1,1));
figure;
subplot(4,1,1);
plot(input);
inputh=((input))*cos(beta);
inputv=((input))*sin(beta);
inputhd=(sqrt(input))*cos(beta);
inputvd=(sqrt(input))*sin(beta);
outputho=conv(inputh,hr11)+conv(inputv,hr21);
```

```
outputvo=conv(inputh,hr12)+conv(inputv,hr22);
outputhod=conv(inputhd,hr11)+conv(inputvd,hr21);
outputvod=conv(inputhd,hr12)+conv(inputvd,hr22);
outputhe=outputho*cos(beta);
outputve=outputvo*sin(beta);
outputee=outputhe+outputve;
subplot(4,1,2);
plot(outputee);
outputd=outputhod.^2+outputvod.^2;
subplot(4,1,3);
plot(outputd(500:1200));
subplot(4,1,4);
eyescat(outputd,10e9/2,10*10e9);
a=randint(Nin-1,1,2);
a=[a'0];
inpute=rcosflt(a,10e9,10*10e9,'normal',1,1);
inputh=((inpute))*cos(beta);
inputv=((inpute))*sin(beta);
outputho=conv(inputh,hr11)+conv(inputv,hr21);
outputvo=conv(inputh,hr12)+conv(inputv,hr22);
outputhe=outputho*cos(beta);
outputve=outputvo*sin(beta);
outpute=outputhe+outputve;
for k=1:Nin
   hh1(k)=outpute(523+10*(k-1));
   hh2(k)=outpute(528+10*(k-1));
end
clear outpute;
inputh=((1))*cos(beta);
inputv=((1))*sin(beta);
outputho=conv(inputh,hr11)+conv(inputv,hr21);
outputvo=conv(inputh,hr12)+conv(inputv,hr22);
outputhe=outputho*cos(beta);
outputve=outputvo*sin(beta);
outpute=outputhe+outputve;
figure;
subplot(4,1,1);
stem(outpute(470:580));

% --------Channel Identification--------
hidenh1=iden(hh1,a);
hidenh2=iden(hh2,a);
len1=length(hidenh1);
```

```
hiden=[];
for k=1:len1
    hidenb=[hidenh1(k) hidenh2(k)];
    hiden=[hiden hidenb];
end
length(hiden);
index_max = find (abs(hiden)== max(abs(hiden)));
hiden=hiden(index_max-2:index_max+3);
hiden=hiden/sqrt(sum(hiden.^2));
subplot(4,1,2);
stem(hiden);
clear hh1;
clear hh2;


% -------Equaliztion Coeffecicents-------
hiden=hiden.';
maxh=find(abs(hiden)==max(abs(hiden)));
D=maxh;
N=12;
wvector=equali(hiden,D,N);
subplot(4,1,3);
stem(conv(hiden',wvector'));
wvector=wvector';
a=[1 zeros(1,1)];
inm=rcosflt(a,10e9,10*10e9,'normal',1,1);
inm=[inm(5) inm(10) inm(15)];
wvector=conv(wvector,inm);
wvector=wvector(1:10);


% ---------10G Converted to 100G----------
subplot(4,1,4);
stem(wvector);
len2=length(wvector);
w=[];
for k=1:len2
    w1=[wvector(k) zeros(1,4)];
    w=[w w1];
end


% -----------PMD Compensation----------
c=conv(outputee,w);
[B,A]=butter(4,0.13);
c=filter(B,A,c);
```

```
figure;
subplot(3,1,1);
plot(c);
subplot(3,1,2);
eyescat(c,10e9/2,10*10e9);


%-------Eye Pattern-------
load Dhr110;
load Dhr120;
load Dhr210;
load Dhr220;
inputh=(sqrt(input))*cos(beta);
inputv=(sqrt(input))*sin(beta);
outputho=conv(inputh,hr11)+conv(inputv,hr21);
outputvo=conv(inputh,hr12)+conv(inputv,hr22);
outputd0=outputho.^2+outputvo.^2;
figure;
subplot(3,1,1);
eyescat(outputd0/10e19,10e9/2,10*10e9);
ylabel('Amplitude (a)');
xlabel(' ');
subplot(3,1,2);
eyescat(outputd,10e9/2,10*10e9);
title(' ');
xlabel(' ');
ylabel('Amplitude (b)');
subplot(3,1,3);
eyescat(c,10e9/2,10*10e9);
ylabel('Amplitude (c)');
title(' ');


%---------Pulse Shape-------------
figure;
subplot(3,1,1);
plot(input);
ylabel('Amplitude (a)');
axis([0 700 -.5 1.5]);
subplot(3,1,2);
plot(outputd(500:1165)/6);
ylabel('Amplitude (b)');
axis([0 700 -.5 1.5]);
subplot(3,1,3);
plot(c(520:1220)/2);
```

```
ylabel('Amplitude (c)');
xlabel('Time [ps]');
axis([0 700 -.5 1.5]);
save  wvec2  w
etime(clock,t0)/60
```

```
function [t,hr,hi]=pmd(fsample,N,deltat,fcutoff)
% This function simulates the impulse response of optical fiber channel with first-order
PMD.
c=2.998e8;
lambda=1550*(1e-9);
foffset=0*c/lambda ;
hf11=1;
hf21=1;
hf12=1;
hf22=1;
K=25;
tk=deltat/(sqrt(K));
r1=rand(1,K);
theta1=pi*2*(r1-0.5);
r2=rand(1,K);
theta2=pi*2*(r2-0.5);
for k=[0:N-1],
c1=1;
c2=1;
f1=k*(fsample/N);
f2=k*(fsample/N)-fsample;
for n=1:K,
a=[exp(j*theta1(n))*cos(theta2(n))   exp(j*theta1(n))*sin(theta2(n))
   -exp(-j*theta1(n))*sin(theta2(n))  exp(-j*theta1(n))*cos(theta2(n))];
b1=[exp(j*tk*pi*(f1+foffset))       0
    0            exp(-j*tk*pi*(f1+foffset))];
b2=[exp(j*tk*pi*(f2+foffset))       0
    0            exp(-j*tk*pi*(f2+foffset))];
c1=c1*a;
c1=c1*b1;
c2=c2*a;
c2=c2*b2;
end
c=c1*rect(f1,fcutoff)+c2*rect(f2,fcutoff);
hf11(k+1)=c(1,1);
hf21(k+1)=c(1,2);
hf12(k+1)=c(2,1);
hf22(k+1)=c(2,2);
end
y(1,:)=hf11;
y(2,:)=hf21;
y(3,:)=hf12;
y(4,:)=hf22;
```

```
ht(1,:)= fsample*ifft(y(1,:));
ht(2,:)= fsample*ifft(y(2,:));
ht(3,:)= fsample*ifft(y(3,:));
ht(4,:)= fsample*ifft(y(4,:));
t=[-N/2:1:(N/2)-1]/fsample;
ht=[ht(:,[N/2+1]:N)   ht(:,[1:N/2])];
hr = real(ht);
hi = imag(ht);
```

```
function hiden=iden(channel_input,a)
% This function obtains the impulse response of optical fiber with PMD by correlation.
pn=(2*(a>0.5)-1);
noise_variance = 0*10^(2) ;
channel_noise = sqrt(noise_variance) * randn(size(channel_input)) ;
channel_output = channel_input + channel_noise ;
reversed_indices = [ length(pn) : -1 : 1 ] ;
matched_filter = conj( pn( reversed_indices ) ) ;
matched_filter_output = conv ( matched_filter , channel_output );
index_max = find (abs(matched_filter_output)== max(abs(matched_filter_output)))
index_max=length(a);
matched_filter_output(index_max);
width_around_max =5;
indices_plot =[ index_max-width_around_max : index_max+width_around_max];
width_around_max1 =100;
indices_plot1 =[ index_max-width_around_max1 : index_max+width_around_max1];
hiden2=matched_filter_output(indices_plot);
hiden1=matched_filter_output(indices_plot1);
hiden=hiden2;
weight=sum(hiden2.^2)/sum(hiden1.^2)
```

```matlab
function wvector = equali( hvector , D , N )
%    This function calculates coefficients of the optical equalizer.
%    wvector are the equalizer taps
%    D is the delay
%    N is the number of taps in w
%    Example:
%    clf
%    h = [0.1 -.5 .2 0 .4].';
%    h = [ 1 1 ].';
%    bitdelay = 15 ;
%    Ntaps = 30 ;
%    wvector = lineareq1 ( h , bitdelay , Ntaps ) ;
%    subplot(2,1,1)
%    stem(wvector)
%    subplot(2,1,2)
%    stem(conv(h,wvector))
uncertainfactor1 =6000;    % training length
uncertainfactor2 = 0.025;   % adaptation parameter
wvector = zeros ( N , 1 ) ;
rvectorshort = wvector ;
Nbits = uncertainfactor1 * max ( [ length(hvector) D N ] ) ;
bvector = 2 * ( rand(Nbits,1) <0.5 ) - 1 ;
rvector = conv2 ( bvector , hvector ) ;
dvector = [ zeros(D,1) ; bvector ] ;
Ntrunc = min([ length(rvector) length(dvector) ])
rvector = rvector([1:Ntrunc]) ;
dvector = dvector([1:Ntrunc]) ;
mu = uncertainfactor2 ;
for i=1:Ntrunc,
    rvectorshort = [ rvector(i) ;
    rvectorshort(1:(length(rvectorshort)-1))] ;
    dhat = (wvector.') * rvectorshort ;
    err= dvector(i) - dhat;
    if i>0.9*Ntrunc
        mu=0.004;
    elseif  i>0.7*Ntrunc
        mu=0.008;
    elseif  i>0.15*Ntrunc
        mu=0.012;
    end
    wvector = wvector + mu * err * rvectorshort ;
end
```

```
% ---------------------- DGD.m ------ ----------------
% This program calculates DGD and searches PSP of the optical channel with PMD.
clear all;
clear figure;
a=[1 0];
[input,t]=rcosflt(a,10e9,10*10e9,'normal',1,1);
figure;
subplot(2,1,1);
plot(input);
load Dhr11;
load Dhr21;
load Dhr12;
load Dhr22;
for n=1:180
mt1=0;
beta=n*pi/(180);
inputh=(sqrt(input))*cos(beta);
inputv=(sqrt(input))*sin(beta);
outputho=conv(inputh,hr11)+conv(inputv,hr21);
outputvo=conv(inputh,hr12)+conv(inputv,hr22);
outpute=outputho.^2+outputvo.^2;
len=length(outpute);
for m=1: len
     mt1=mt1+m*(outpute(m)^2);
end
mt2=sum(outpute.^2);
mt=mt1/mt2;
icenter(n)=mt;
end
alpha1=find(max(abs(icenter))==abs(icenter));
alpha2=find(min(abs(icenter))==abs(icenter));
dgd=max(icenter)-min(icenter)
alpha1
alpha2
subplot(2,1,2);
plot(outpute);
```